ACS NANO

www.acsnano.org

ARTICLE

Targeted Carbon Nanostructures for Chemical and Gene Delivery to Plant Chloroplasts

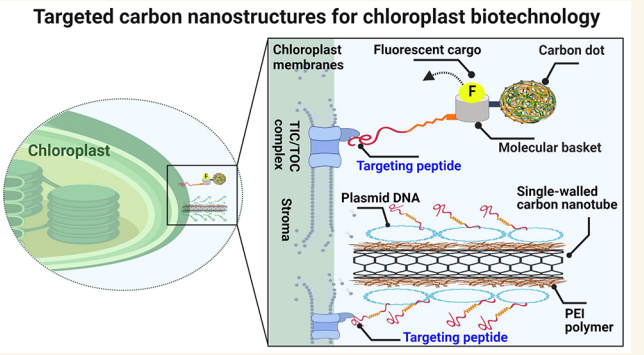
Israel Santana, Su-Ji Jeon, Hye-In Kim, Md Reyazul Islam, Christopher Castillo, Gail F. H. Garcia, Gregory M. Newkirk, and Juan Pablo Giraldo*

Cite This: *ACS Nano* 2022, 16, 12156–12173

Read Online

ACCESS | Metrics & More | Article Recommendations | Supporting Information

ABSTRACT: **Nanotechnology approaches for improving the delivery efficiency of chemicals and molecular cargoes in plants through plant biorecognition mechanisms remain relatively unexplored. We developed targeted carbon-based nanomaterials as tools for precise chemical delivery (carbon dots, CDs) and gene delivery platforms (single-walled carbon nanotubes, SWCNTs) to chloroplasts, key organelles involved in efforts to improve plant photosynthesis, assimilation of nutrients, and delivery of agrochemicals. A biorecognition approach of coating the nanomaterials with a rationally designed chloroplast targeting peptide improved the delivery of CDs with molecular baskets (TP-β-CD) for delivery of agrochemicals and of plasmid DNA coated SWCNT (TP-pATV1-SWCNT) from 47% to 70% and from 39% to 57% of chloroplasts in leaves, respectively. Plants treated with TP-β-CD (20 mg/L) and TP-pATV1-SWCNT (2 mg/L) had a low percentage of dead cells, 6% and 8%, respectively, similar to controls without nanoparticles, and no permanent cell and chloroplast membrane damage after 5 days of exposure. However, targeted nanomaterials transiently increased leaf H_2O_2 (0.3225 μmol gFW^{-1}) above control plant levels (0.03441 μmol gFW^{-1}) but within the normal range reported in land plants. The increase in leaf H_2O_2 levels was associated with oxidative damage in whole plant cell DNA, a transient effect on chloroplast DNA, and a decrease in leaf chlorophyll content (−17%) and carbon assimilation rates at saturation light levels (−32%) with no impact on photosystem II quantum yield. This work provides targeted delivery approaches for carbon-based nanomaterials mediated by biorecognition and a comprehensive understanding of their impact on plant cell and molecular biology for engineering safer and efficient agrochemical and biomolecule delivery tools.**



KEYWORDS: *agrochemical delivery, gene delivery, chloroplast biotechnology, peptides, smart agriculture, nanomaterial−plant interactions*

Downloaded via UNIV OF CALIFORNIA RIVERSIDE on August 31, 2022 at 20:59:38 (UTC).
See https://pubs.acs.org/sharingguidelines for options on how to legitimately share published articles.

The increasing demand for food production requires innovative and sustainable technologies for efficient agrochemical and biomolecule delivery in plants. Human population growth is expected to require a 60% increase or more in food production by 2050 relative to 2005−2007 levels.[1] Traditional plant breeding, genetic engineering, and land management strategies are not on track to meet the need for increased food production.[2,3] Climate change will further complicate efforts toward achieving food security by exacerbating the frequency and intensity of environmental stresses that negatively impact crop productivity.[4,5] The higher demand for higher crop yields is straining the earth's ecosystems by increasing energy, water, land use, and environmental pollution.[6,7] The transition to sustainable food production systems will require innovations in agrochemical delivery and genetic engineering strategies. Nanotechnology is emerging as a tool to improve sustainable agricultural practices and maintain food security during a rapidly increasing human population and the threat of climate change impact on crop yields.[8−10]

Nanotechnology is providing approaches for more precise agrochemical delivery, genetic engineering platforms, and environmental sensing for enabling farmers to monitor, manage, and improve crop productivity.[3,8,10−13] The use of engineered nanomaterials in agriculture relies on both advancing our fundamental understanding of nanomaterial−plant interactions and elucidating the impact of nanomaterials on plant function. Nanotechnology applications without

Received: March 18, 2022
Accepted: August 4, 2022
Published: August 9, 2022



© 2022 American Chemical Society

https://doi.org/10.1021/acsnano.2c02714
ACS Nano 2022, 16, 12156−12173

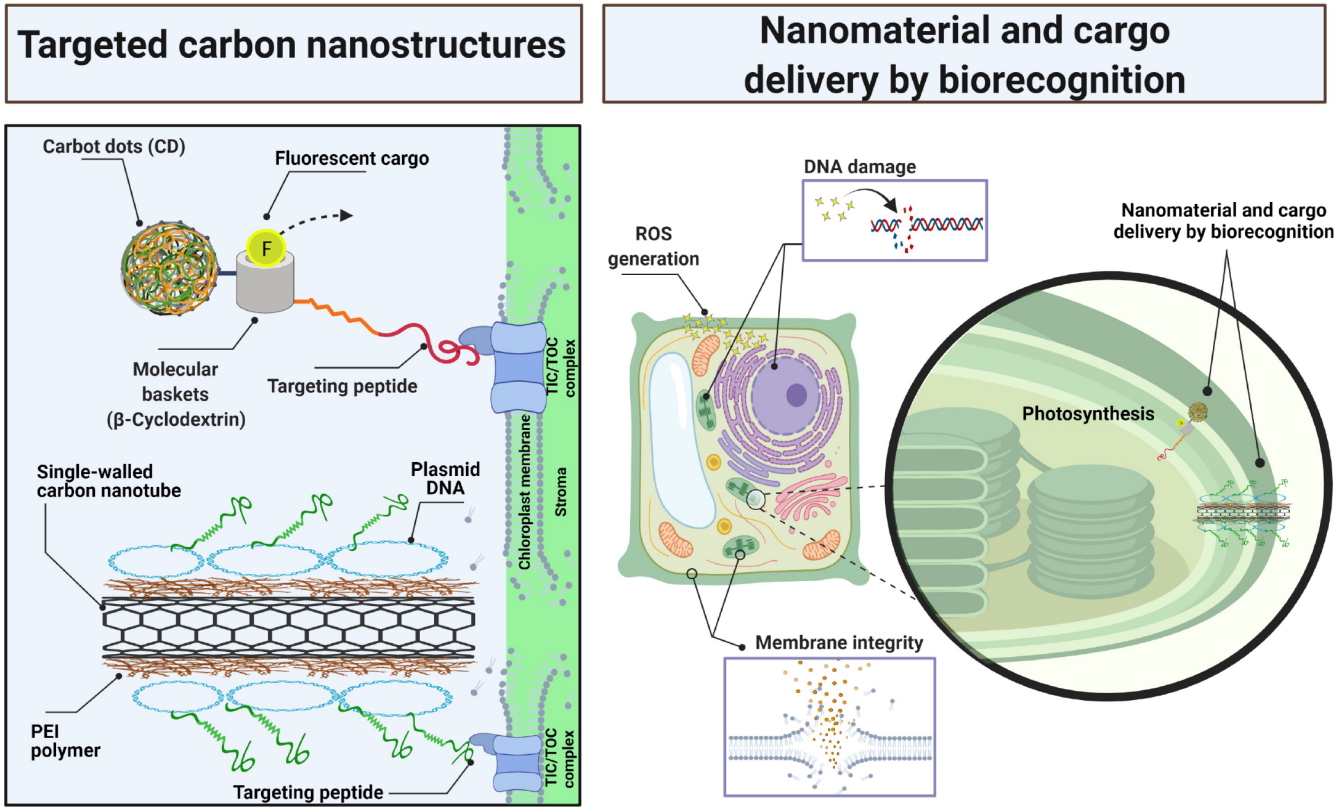


Figure 1. Targeted carbon nanostructures for chloroplast bioengineering and their impact on the plant cell and molecular biology. Nanomaterials were synthesized for chloroplast targeted chemical delivery (CDs) and gene delivery (SWCNTs). The carbon nanostructures were functionalized with a guiding peptide that selectively binds to protein translocon outer channels (TOC) on the chloroplast membrane. Nanomaterials have been proposed to spontaneously enter plant cells and organelles by disrupting lipid bilayers. The impact of targeted carbon nanostructures on leaf cell and molecular biology was assessed by studying the effects on plant cell and chloroplast membrane integrity, the damage to whole plant cell and isolated chloroplast DNA, the generation of ROS, and photosynthesis. Created with BioRender.com.

adequately evaluating the biological impact on plant function can lead to unforeseen plant health and environmental consequences, causing decreased crop yield and pollution of the environment.[10,14,15] Therefore, studies on the design of nanomaterials should go hand in hand with research on their biocompatibility with plants.

Nanomaterials exhibit tunable physical and chemical properties such as size, surface charge, amphiphilicity, and biomolecule coatings that enable targeted and controlled delivery of chemicals and biomolecules.[16−20] Targeted delivery through nanomaterials in agriculture has gained interest due to its tremendous potential for improving pesticide, herbicide, and fertilizer delivery while decreasing the environmental impact due to agrochemical runoff.[3,9,10,16,21] Current approaches for improving the delivery efficiency of nanomaterials and their cargoes in plants have been based on modifications of the nanoparticle charge, size and hydrophobicity.[18−20,22−24] The use of biomolecule coatings to guide nanomaterials to plant cells and organelles by the plant biorecognition machinery has only been recently explored and remains poorly understood.[16,25] For example, Santana et al. recently demonstrated that quantum dots functionalized with a highly conserved chloroplast targeting peptide among dicot plants could deliver nanomaterials with chemical cargoes inside ∼75% of chloroplasts in leaf cells and modulate chloroplast redox status.[16,26] These CdSe quantum dots were used for fundamental research on plant-nanoparticle interactions because long-term exposure to cadmium-based nanomaterials can be toxic to plants and the environment.[27] Quantum dots are model nanomaterials for understanding plant−nanoparticle interactions that can be traced by multiple advanced analytical tools including confocal fluorescence microscopy and elemental analysis, but they are not suitable for nanoenabled agriculture applications due to their toxicity.[27,28] In contrast, carbon dots (CDs) are among the most biocompatible[29−31] and degradable nanomaterials[31,32] made from renewable resources such as citric acid and urea.[18,33] Functionalizing CDs with molecular baskets (β-cyclodextrins) able to carry a wide range of agrochemicals[16,34,35] and targeting peptides allow them to act as sustainable targeted chemical delivery tools for agricultural applications.

Nanomaterials are also promising genetic engineering platforms due to their ability to bypass plant cell barriers including the cell wall and lipid membranes without mechanical aid in a broad array of plant species, including some recalcitrant to conventional genetic engineering approaches.[9,11,19,24,36] High aspect ratio nanomaterials functionalized with highly positively charged polymers have been reported to enable the delivery of genetic elements into plants nuclear and chloroplast genomes.[11,19,37,38] The delivery of a DNA plasmid encoding a green fluorescent protein (GFP) to the plant nuclear genome was mediated by single-walled carbon nanotubes (SWCNTs) that were covalently modified with a cationic polymer (polyethylenimine, PEI).[24,37] The

https://doi.org/10.1021/acsnano.2c02714
ACS Nano 2022, 16, 12156−12173

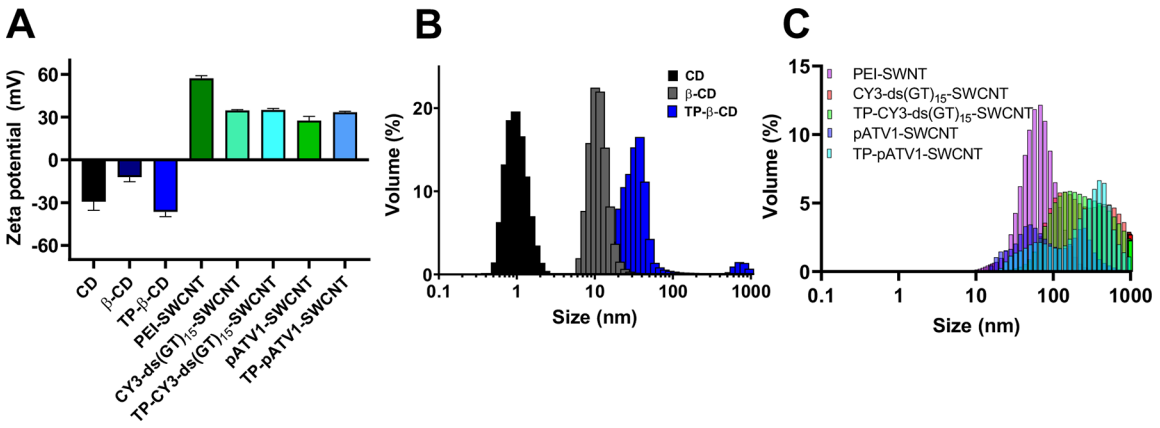


Figure 2. Characterization of carbon nanostructures for chemical and gene delivery to chloroplasts. (A) ζ potential and (B, C) hydrodynamic diameter of targeted and nontargeted carbon nanostructures. CDs with β-cyclodextrin molecular baskets (β-CDs) and chloroplast targeting peptides (TP-β-CDs). PEI-SWCNTs coated with pATV1 plasmid DNA (pATV1-SWCNT), CY3-ds(GT)$_{15}$-SWCNT and nanostructures with chloroplast targeting peptide (TP-pATV1-SWCNT, TP-CY3-ds(GT)$_{15}$-SWCNT).

surface functionalization with positively charged PEI allowed electrostatic interactions with the negatively charged plasmid DNA cargoes and the transport across plant cell barriers including the cell wall and plasma membrane. Passive delivery of plasmid DNA without mechanical aid was confirmed by expression analysis of GFP using digital drop PCR and confocal imaging in live plant cells. Furthermore, Kwak et al. reported the delivery of plasmid DNA encoding a yellow fluorescent protein into chloroplasts by chitosan-coated SWCNTs and assessed expression by confocal microscopy analysis.[19] These studies investigated plasmid DNA delivery to chloroplasts by tuning the SWCNT surface charge with polymers. However, biorecognition approaches for targeting plasmid DNA via SWCNTs have not been explored. There is also a need to determine the biocompatibility of these carbon nanostructures and their impact on plant cell and organelle function for plant genetic engineering applications.

Studies on CDs and SWCNTs impact on plants and the environment tend to be performed after plant exposure to high doses of nanomaterials, >100 mg/L and >25 mg/L, respectively.[14,39] The studies on interactions between carbon-based nanomaterials and plants have mainly focused on nanomaterials delivered through hydroponic, soil, and agar substrates[29,40,41] but not by foliar delivery approaches. Mechanistic studies are needed to determine the effect of targeted carbon nanomaterials within a range of concentrations intended for plant biotechnology and agricultural systems.[39,42] Biological impact studies provide insights into designs and synthesis of nanomaterials that do not negatively affect plant growth and development.[39] Understanding the effect that targeted nanomaterials have on plant cell and molecular biology is critical toward engineering safer and effective chemical and biomolecule delivery strategies.

This study developed nanocarriers for targeted delivery of chemicals and plasmid DNA to chloroplasts using carbon-based nanomaterials and investigated the impact of these nanocarriers on plant cell and molecular biology (Figure 1). The targeted CDs contained a β-cyclodextrin molecular basket able to form inclusion complexes with chemical cargos[16,34,35] and a targeting peptide (TP) from the rubisco small subunit 1A that improves binding and uptake by chloroplasts (TP-β-CD). The SWCNT functionalized with cationic polymers electrostatically bound to plasmid DNA driven by a plastid-specific promoter (pATV1)[43] and to a chloroplast targeting peptide are shown to act as a targeted gene delivery platform (TP-pATV1-SWCNT). We show proof of concept that these carbon nanostructures target the delivery of a fluorescent chemical cargo and plasmid DNA through confocal fluorescence microscopy and molecular analysis. We investigated the impact of targeted nanomaterials on percentage of viable leaf cells, cell and plastid membrane intactness, leaf cell H_2O_2 levels, oxidative damage to DNA, chlorophyll, and photosynthesis. This work provides a comprehensive understanding of the interactions of targeted carbon nanostructures with cargoes in plants and their impact on plant cell, organelle, and molecular biology.

RESULTS AND DISCUSSION

Targeted Carbon Nanomaterials for Chemical and Gene Delivery. The UV−vis absorbance spectrum of targeted CDs indicated characteristic absorption peaks at 272 nm for $\pi-\pi$ transition of C═C bonds and 335 nm for n−π* transition of C═O or C═C bonds, respectively (Figure S1).[44−46] Nontargeted PEI coated single-walled carbon nanotubes (PEI-SWCNTs) showed absorption peak shoulders around 260 nm due to the PEI polymer (Figure S1).[47] Both CD and TP-pATV1-SWCNT absorbance spectra broadening at 215−350 nm range are attributed to the surface functionalization with biomolecules such as peptides, DNA or β-cyclodextrin.[48,49,46] The ζ potential of β-CD (−12.1 ± 3.2 mV) decreased after functionalization with the chloroplast targeting peptide in TP-β-CD (−36.4 ± 3.4 mV) (10 mM TES buffer, pH 7.0) (Figure 2A). The chloroplast targeting peptide for CD (MASSMLSSATMVGGC) has a neutral charge (−0.1 mV) that upon covalent bonding to positively charged NH_2 groups in β-cyclodextrins through a NHS-PEG4-MAL linker results in the decrease in ζ potential for TP-β-CD. The ζ potential for PEI-SWCNT decreased from 57.3 ± 1.9 mV to 33.4 ± 0.76 mV for targeting peptide coated TP-pATV1-SWCNT (10 mM TES and 0.1 mM NaCl, pH 7.0) (Figure 2A). The electrostatic interactions between the negatively charged plasmid DNA (pATV1) and the positively charged PEI on the SWCNT surface decrease the ζ potential of TP-pATV1-SWCNT. The CY3-ds(GT)$_{15}$-SWCNT and TP-CY3-ds(GT)$_{15}$-SWNT had similar ζ potentials of 34.6 ± 0.6 and 35.1 ± 0.9 mV, respectively (Figure 2A). The hydrodynamic

https://doi.org/10.1021/acsnano.2c02714
ACS Nano 2022, 16, 12156−12173

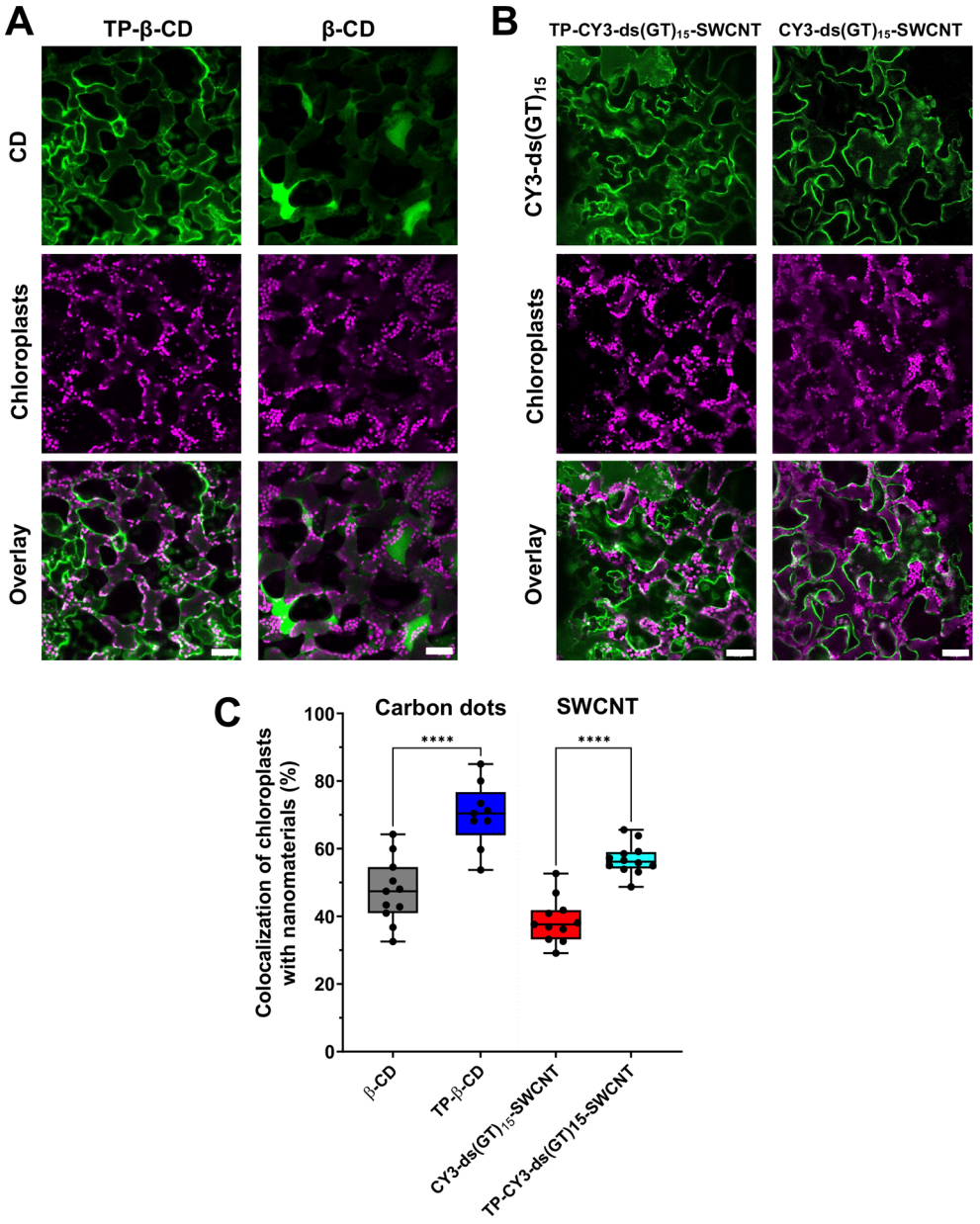


Figure 3. Targeted delivery of nanomaterials to chloroplasts in plant cells. (A) Confocal microscopy images of CDs with β cyclodextrin molecular baskets (β-CDs) and chloroplast targeting peptides (TP-β-CDs) and (B) single walled carbon nanotubes coated with CY3 with double-stranded DNA (CY3-ds(GT)$_{15}$-SWCNT) and chloroplast targeting peptides (TP-CY3- ds(GT)$_{15}$-SWCNT). Confocal images were collected in the same focal plane about 50 μm from the leaf abaxial epidermis. Scale bar 50 μm. (C) Colocalization analysis of nanostructures indicated a significantly higher percentage of chloroplasts with targeted nanomaterials compared to controls without TPs. Statistical analysis using a one-way ANOVA and post hoc Tukey's test, $n = 7-12$, ****$p < 0.0001$.

size for CY3-ds(GT)$_{15}$-SWCNT and TP-CY3-ds(GT)$_{15}$-SWCNT was also similar, 221.8 ± 13.02 nm and 216.7 ± 8.23 nm, respectively (Figure 2C). Both targeted TP-β-CDs and TP-pATV1-SWCNTs have a highly negative or positive charge, respectively, that has been shown to promote uptake through chloroplast envelopes and plasma membranes in vitro[23] and leaf biosurfaces in vivo.[18] The hydrodynamic size for β-CD measured by dynamic light scattering increased from 10.2 ± 1.5 nm to 27.8 ± 5.8 nm for TP-β-CD (Figure 2B). Likewise, the average DLS size for the pATV1-SWCNT and TP-pATV1-SWCNT increased from 49.98 ± 3.45 nm to 382.5 ± 27.0 nm, respectively (Figure 2C). The increase in DLS size is associated with the coating of pATV1-SWCNT with a modified chloroplast targeting peptide (30 residues, MASSMLSSATMVGGGGGGKHKHKHKHKHKH).

The Fourier-transform infrared spectroscopy (FTIR) analysis of CDs indicated characteristic bonds for O−H stretching vibrations at 3240 cm^{-1}, C≡C alkyne 2160 cm^{-1}, carboxamides N═C═N at 2010 cm^{-1}. The peaks near 1700 cm^{-1} and 1650 cm^{-1} were attributed to C═O conjugated aldehydes and N−H amine bonds[33,50] (Figure S2). The β-CDs exhibited significant characteristic peaks for asymmetric glycosidic vibration bonds (C−O−C) of β-cyclodextrins at 1040 cm^{-1} (Figure S2).[33,51] The FTIR of targeted TP-β-CDs exhibited peaks at O−H stretching vibrations at 3240 cm^{-1}, asymmetric glycosidic vibration (C−O−C) at 1050 cm^{-1}, and bands typical of type I amide bonds at 1610 cm^{-1}, supporting

https://doi.org/10.1021/acsnano.2c02714
ACS Nano 2022, 16, 12156−12173

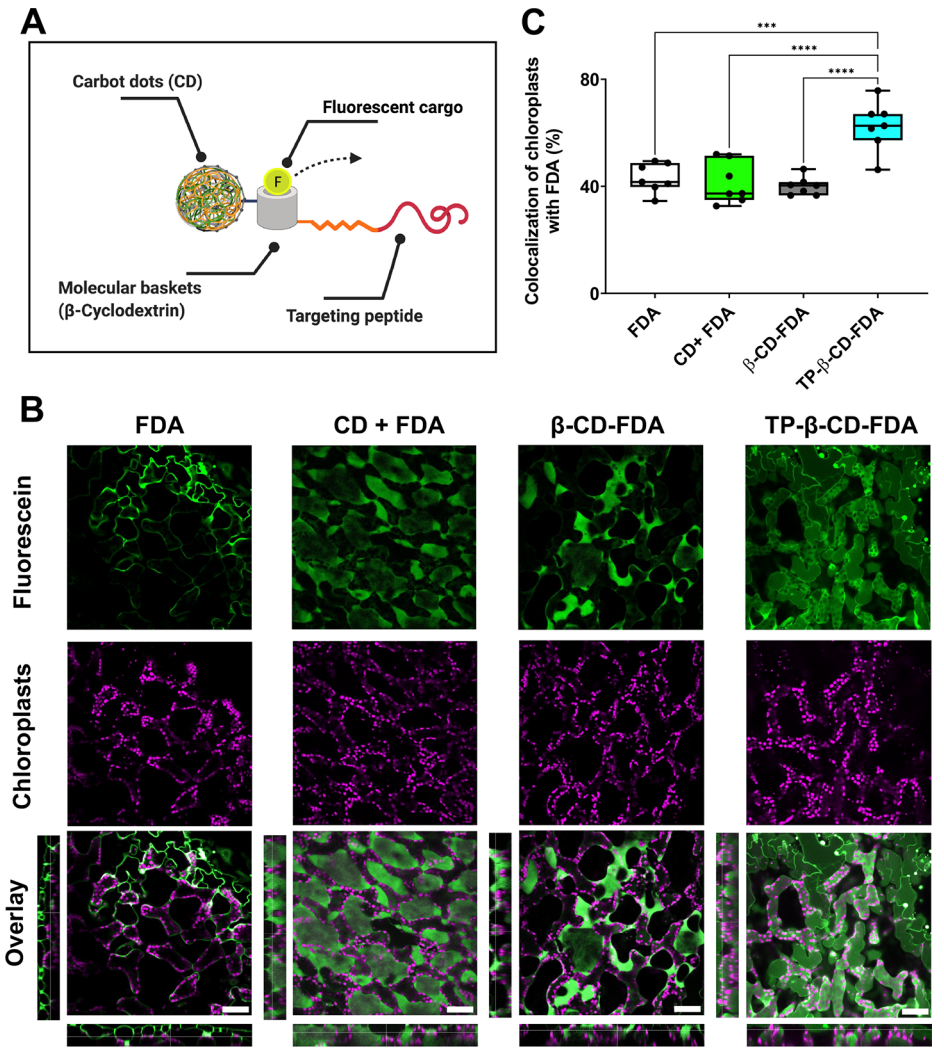


Figure 4. Chemical cargo delivery by targeted CD nanostructures. (A) CDs are functionalized with a *β*-cyclodextrin molecular baskets for chemical cargo delivery (e.g., fluorescent dye) and with chloroplast guiding peptide for targeted delivery enabled by biorecognition. (B) Confocal microscopy images of fluorescein (FDA) in leaf mesophyll cells indicate a higher degree of colocalization with chloroplasts for targeted TP-*β*-CD-FDA compared to nontargeted *β*-CD-FDA, FDA alone, or a mixture of CDs and FDA. Merged confocal images show 2D Z-projections to visualize the distribution of fluorescent cargoes in leaf mesophyll cells and chloroplasts. Confocal images were collected in the same focal plane about 50 *μ*m from the leaf abaxial epidermis. Scale bar 50 *μ*m. (C) Quantitative colocalization analysis of the percentage of chloroplasts containing FDA. Statistical analysis was performed using a one-way ANOVA and post hoc Tukey's test, $n = 7$, *** $p < 0.0002$, **** $p < 0.0001$.

the successful conjugation of *β*-cyclodextrin and targeting peptides on the CD surface (Figure S2). The CDs exhibited a fluorescence emission peak at 511 nm, and the SWCNTs coated in CY3-ds$(GT)_{15}$ DNA showed a fluorescence emission peak at 564 nm. These nanomaterial fluorescence peaks of emission allowed tracking inside plant cells with minimum overlap with chloroplast autofluorescence background (Figure S1).

In Vivo Imaging of Chloroplast Targeted Nanomaterials. Confocal fluorescence microscopy imaging was used to determine the colocalization between chloroplasts in *Arabidopsis* leaves and both targeted and nontargeted *β*-CDs and CY3-ds$(GT)_{15}$ DNA coated SWCNT (Figure 3A,B). Nanomaterials were foliar sprayed on whole plants in a formulation containing 0.1% Silwet (v/v) (Table S1). Control confocal images of leaves treated with only 10 mM TES buffer have no background autofluorescence in CD and CY3-ds$(GT)_{15}$ DNA emission channels (Figure S3). The level of colocalization of fluorescent emission from nanocarriers with chloroplasts was determined by Manders' coefficient analysis (COLOC2, ImageJ) (Figure 3C). The localization of targeted nanomaterials (TP-*β*-CD and TP-CY3-ds$(GT)_{15}$-SWCNT) with chloroplasts in leaf mesophyll cells was higher compared to nontargeted materials lacking the targeting peptide (*β*-CD and CY3-ds$(GT)_{15}$-SWCNT). The colocalization rates for TP-*β*-CDs with chloroplasts significantly increased to 70.0 ± 9.46% from 47.4 ± 9.57% levels for *β*-CDs and similarly to 56.9 ± 4.58% for TP-CY3-ds$(GT)_{15}$-SWCNT from 38.7 ± 6.69% for CY3-ds$(GT)_{15}$-SWCNT ($p < 0.0001$) (Figure 3C). Previously, we reported an in vivo increase in colocalization of chloroplasts with heavy-metal-based quantum dots functionalized with chloroplast targeting biorecognition peptides,[16] indicating the robustness of this approach for a variety of targeted nanomaterials. The use of foliar delivery of nanomaterials onto leaves provides a facile, efficient, and scalable method to interface nanomaterials with crops.[21,52] Foliar

https://doi.org/10.1021/acsnano.2c02714
ACS Nano 2022, 16, 12156−12173

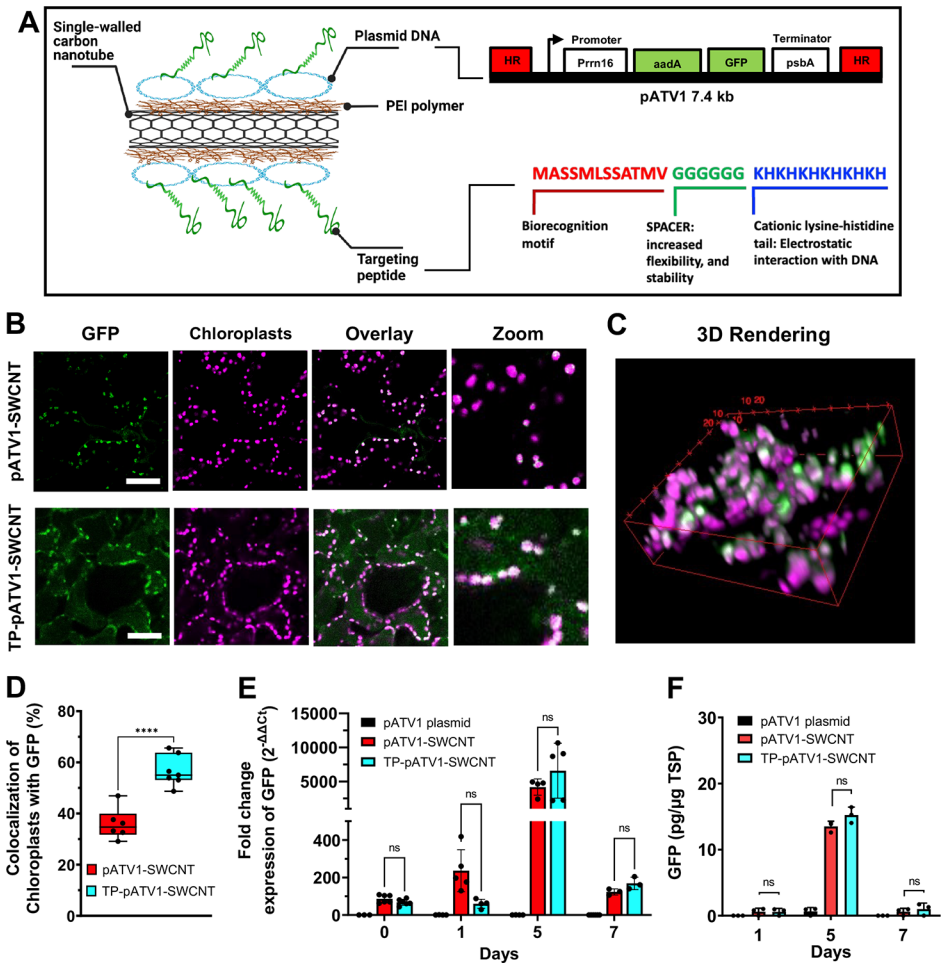


Figure 5. Plasmid DNA delivery to chloroplasts by targeted SWCNTs. (A) SWCNTs coated with PEI are electrostatically bound to plasmid DNA and chloroplast targeting peptides for chloroplast genetic engineering. The pATV1 plasmid encodes for a GFP gene. The chloroplast targeting peptide was rationally designed to include amino acid sequences for biorecognition, increased flexibility and stability, and an electrostatic tail to bind to DNA. (B) Confocal microscopy images of *Arabidopsis thaliana* leaf mesophyll cells after 7 days of exposure to SWCNTs coated in pATV1 plasmid with targeting peptides (TP-pATV1-SWCNTs) and without the guiding peptides (pATV1-SWCNTs). Scale bar 50 μm. (C) 3D image of GFP in leaf mesophyll cells after treatment with TP-pATV1-SWCNT. (D) Quantitative colocalization analysis of chloroplasts with GFP fluorescence. Comparisons were performed by independent samples *t*-test (two-tailed, ****p = < 0.0001, n = 5−7). (E) RT-qPCR gene expression analysis of GFP in plants treated with targeted TP-pATV1-SWCNTs and nontargeted pATV1-SWCNTs. Data are the means ± SD (n = 5−7). (F) ELISA quantification of GFP in total soluble proteins of extracts from leaves treated with targeted TP-pATV1-SWCNTs and nontargeted pATV1-SWCNT. Data are means ± SD (n = 3). Statistical analysis was performed with a two-way ANOVA. No significant differences (ns).

chemical delivery approaches mediated by nanomaterials in plants can improve the efficacy of fertilizer, pesticides, and other agrochemicals for enhancing plant growth.

The colocalization of TP-β-CDs and TP-CY3-ds$(GT)_{15}$-SWCNTs with chloroplast inside leaf mesophyll cells indicates that these nanomaterials are able to translocate across the leaf surface and through plant cell barriers including the cell wall, plasma membrane, and chloroplast envelopes. The nanomaterial uptake pathway is likely micron-sized stomatal pores through which we have reported the translocation of CDs in crop leaves.[18] Although, stomatal density is lower on the upper (adaxial) leaf surface than on the lower (abaxial) side in *Arabidopsis* as in most plants, the high levels of colocalization of nanomaterials with chloroplasts indicate that this does not constitute a limitation for the translocation of the nanomaterials through plant cell barriers. The larger size of the TP-β-CDs and TP-CY3-ds$(GT)_{15}$-SWCNTs compared to their untargeted counterparts does not decrease their ability to translocate across plant cell barriers and reach the chloroplast target. To the contrary, the coating with targeting peptide biorecognition motifs improved the delivery efficiency to chloroplasts. These results indicate that more research is needed to understand how biomolecule coatings affect the permeability of nanomaterials through plant cell walls reported to act as size exclusion barriers for nanoparticles.[53] The ζ potential of TP-β-CDs and TP-CY3-ds$(GT)_{15}$-SWCNTs was higher in magnitude than 30 mV, which has been predicted by nanoparticle-interactions models to allow delivery of nanomaterials into chloroplasts in vitro.[18,22,23] Previous studies have also reported that highly charged CDs and nanotubes move across leaf cell barriers into chloroplasts in vivo.[18,54]

Chemical Cargo and Plasmid DNA and Delivery to Chloroplasts Mediated by Targeted Nanomaterials. To assess the delivery of chemical cargoes to chloroplasts mediated by TP-β-CD nanocarriers, we loaded β-cyclodextrins with the fluorescent dye 6-carboxyfluorescein (FDA) (Figure

https://doi.org/10.1021/acsnano.2c02714
ACS Nano 2022, 16, 12156−12173

4A). We imaged the localization of FDA within leaf mesophyll tissues by confocal microscopy and quantified the localization of this fluorescence dye with chloroplasts autofluorescence (Figure 4B,C). Plant leaves treated with TP-β-CD-FDA or TP-β-CD (Table S1) were analyzed for the fluorescence emission crosstalk with confocal microscopy under laser excitation with a 488 nm laser (Figure S4A). FDA dye emission spectra exhibited a much stronger fluorescence signal compared to TP-β-CDs at 488 nm excitation allowing detection of loaded cargos to chloroplasts with a minimal crosstalk from TP-β-CDs emission (Figure S4B). The FDA alone localized near the plasma membrane. When added together with CDs or β-CDs, the FDA was observed both in the intracellular and extracellular space. As shown in 2D plane projections in the *XZ* and *YZ* axis from orthogonal Z-stack images (Figure 4B), the FDA delivered by CD + FDA and β-CD-FDA localized with a fraction of chloroplasts at a colocalization rate of 44.5 ± 6.4 and 47.0 ± 9.6%, respectively. In contrast, when FDA was delivered by TP-β-CDs, most of the FDA fluorescence signal was detected inside leaf mesophyll cells and highly colocalized with chloroplasts (70.0 ± 9.5%) (Figure 4B). Using the 2D plane Z-projections, we confirmed this distribution analysis of FDA in the leaf mesophyll and the localization with chloroplasts (Figure 4B). Despite that the TP-β-CD DLS size is larger than their nontargeted counterparts (Figure 2B), these nanocarriers more efficiently deliver chemical cargo to chloroplasts, indicating that their high ζ potential (>30 mV) and targeting peptide coating play a more important role in determining their translocation efficiency through leaf mesophyll cells. Although targeted TP-β-CDs improved the delivery of FDA to chloroplasts in leaf mesophyll cells, the FDA fluorescence signal was localized throughout the entire leaf mesophyll cells. This might indicate that the FDA cargo was also released inside the cell cytosol before reaching chloroplast target organelles. The β-cyclodextrin surface chemistry can be modified for controlled release of cargoes (i.e., pH),[55] providing a pathway to more efficiently deliver the chemical cargo to the intended target. Colocalization rates of FDA fluorescence with chloroplasts were determined using Mander's coefficient analysis (COLOC2, ImageJ). The colocalization rates of TP-β-CDs loaded with FDA were compared to FDA dye only, core CDs mixed with FDA, and β-CDs loaded with FDA (Figure 4C). The percent localization of FDA delivered by TP-β-CDs (62.5 ± 9.22%) was significantly higher compared to nontargeted β-CDs (40.0% ± 3.42) (*** $p < 0.0002$, **** $p < 0.0001$) (Figure 4C). Targeted delivery to chloroplasts by TP-β-CDs provides a traceable fluorescent nanotechnology-based tool with biocompatibility[18,56] and degradability[32,57,58] for agrochemical delivery in plants with improved subcellular delivery precision and cell uptake efficiency. The development of targeted chemical delivery approaches in plants can aid in improving the efficacy of agrochemical delivery while minimizing unintended pollution in the environment.[21,59]

We investigated the targeted delivery of plasmid DNA and expression in chloroplasts of *Arabidopsis* leaves mediated by biorecognition of SWCNTs. We used pATV1, a dicistronic plasmid encoding for both a GFP and antibiotic resistance genes regulated by a chloroplast promoter that is codon-optimized for specific expression in chloroplasts (Figure 5A).[43] The pATV1-SWCNTs were coated with a modified chloroplast targeting peptide (MASSMLSSATMVGGGGGGKHKHKHKHKHKH) that contains a 15 lysine and histidine residues (KH_6) tail. The KH_6 peptide tail enables the electrostatic binding of the chloroplast targeting peptide to the negatively charged plasmid DNA in pATV1-SWCNTs, and the G_6 spacer enhances the exposure of the biorecognition motif to chloroplast membrane receptors.[60−62] The GFP fluorescence was imaged by confocal microscopy in leaf mesophyll cells (Figure 5B). A 3D rendering of GFP expression and chloroplasts autofluorescence indicated high levels of GFP in these organelles in selected leaf mesophyll cells treated with targeted TP-pATV1-SWCNTs (Figure 5C). Confocal analysis of GFP fluorescence emission in plant leaves treated with TP-pATV1-SWCNTs exhibited a more robust GFP signal and higher colocalization within chloroplast in vivo (56.7 ± 6.0%) than nontargeted pATV1-SWCNTs (37.0 ± 6.3%) (Figure 5D). Despite that TP-pATV1-SWCNTs have a larger DLS size than their nontargeted counterparts and similar ζ potential (Figure 2A,B), the targeting peptide coated nanocarriers more efficiently deliver DNA to chloroplasts, indicating that biorecognition mechanisms exert a stronger influence on their translocation through leaf biosurfaces. No background fluorescence was detected in the GFP emission range when *Arabidopsis* plants were treated with only PEI coated SWCNTs (Figure S5).

Expression analysis results indicated that the peak of mRNA transcription levels for GFP is reached after 5 days of exposure for either TP-pATV1-SWCNT or pATV1-SWCNT, which is followed by a decrease in GFP gene expression at day seven (Figure 5E). Interestingly, despite higher localization of targeted TP-pATV1-SWCNTs with chloroplasts, both TP-pATV1-SWCNTs and pATV1-SWCNTs exhibited similar levels of GFP mRNA. This indicates that functionalization of plasmid DNA coated SWCNTs with targeting peptides increases localization with chloroplasts, but it may lead to interference with the plasmid DNA expression by chloroplasts. An alternative explanation is that the targeted TP-pATV1-SWCNTs cause higher rupturing of the chloroplast membranes (as demonstrated in experiments below), thus decreasing overall gene expression in the chloroplasts. The RT-qPCR analysis of GFP mRNA expression was compared to the relative change in expression of the internal housekeeping gene Actin2 (AT3G18780).[63,64] GFP expression was also confirmed by quantifying GFP protein levels with an ELISA assay of the total soluble proteins of leaf extracts. Maximum levels of GFP protein were detected in the total soluble proteins after 5 days of treating leaves with both TP-pATV1-SWCNT and pATV1-SWCNT, followed by a reduction in GFP levels at day 7 (Figure 5F). This additional quantitative analysis mirrors the trend observed in RT-qPCR GFP gene expression (Figure 5E) and provides an orthogonal line of evidence of GFP production by chloroplasts. SWCNTs functionalized with positively charged chitosan have been reported to deliver plasmid DNA to chloroplasts in plant leaves where gene expression was assessed by confocal fluorescence microscopy.[19] Herein, we report that biorecognition-mediated delivery of plasmid DNA to chloroplasts by targeted SWCNT enables high levels of transient transgene expression using confocal microscopy, quantitative gene expression and protein level analysis.

Impact of Targeted Nanomaterials on Plant Cell Viability. We investigated the viability of plant cells treated with increasing concentrations of targeted and nontargeted nanomaterials by measuring the percentage of dead plant cells. *Arabidopsis* leaf tissues were treated with targeted nanomateri-

https://doi.org/10.1021/acsnano.2c02714
ACS Nano 2022, 16, 12156−12173

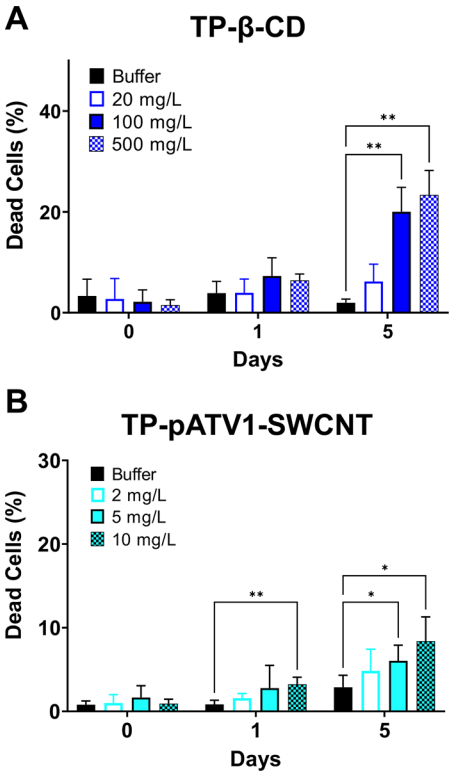


Figure 6. Biocompatibility of targeted nanomaterials in plant cells. Percentage of dead cells in *Arabidopsis* leaf mesophyll tissue exposed to increasing concentrations of targeted nanomaterials. (A) TP-β-CDs or (B) TP-pATV1-SWCNTs. The percentage of dead cells was determined using PI, a fluorescent dye that stains the nuclei of dead cells. Statistical analysis using one-way ANOVA and post hoc Dunnett's test, n = 7−12,*p < 0.032, **p = <0.0021.

als at 20, 100, 500 mg/L concentrations of TP-β-CDs or 2, 5, 10 mg/L of TP-pATV1-SWCNTs (Figure 6, Table S1). Biocompatibility assays were performed up to 5 days of nanocarrier exposure before control *Arabidopsis* plants experienced the onset of leaf senescence marked by significant changes in chlorophyll levels (Figure S6A). On day 7, significant differences in chlorophyll were detected in control *Arabidopsis* plants without nanomaterials. The percentage of intact cells at day 1 for TP-β-CDs (20 mg/L) and TP-pATV1-SWCNTs (2 mg/L) was biocompatible, resulting in no significant differences in plant dead cells relative to controls without nanoparticles over the same experimental time frame (Figure 6A,B). However, the TP-β-CDs exhibited significantly higher percentages of dead cells on day 5 of exposure at concentrations of 100 mg/L (20.0 ± 4.8%) and 500 mg/L (23.4 ± 4.8%) compared to controls (2.0 ± 0.7%) (Figure 6A). Similarly, the TP-pATV1-SWCNT treated leaves showed an increase in cell death on day 5 at concentrations of 5 mg/L (6.0 ± 1.9%) and 10 mg/L (8.4 ± 2.9%) relative to controls (2.9 ± 1.4%) (Figure 6B). Therefore, subsequent experiments assessing the impact of targeted nanocarriers on plant cell and molecular biology were focused on biocompatible concentrations of 20 mg/L for TP-β-CDs and 2 mg/L for TP-pATV1-SWCNTs.

Interactions of Targeted Carbon Nanostructures with Plant Cell and Chloroplast Membranes. Damage to plant lipid membranes causes ion and molecule permeability changes across the membrane, interruption of metabolic processes, intracellular signaling, and trafficking of biomolecules.[65,66] The application of targeted nanostructures with high charge allows penetration of plant cell barriers and localization inside organelles that could cause disruption in lipid membrane integrity. Plant cell membrane intactness in leaves treated with TP-β-CDs or TP-pATV1-SWCNTs (Table S1) was assessed by staining dead cells with propidium iodide (PI) dye followed by imaging under confocal microscopy (Figure 7A). PI is a nonpermeable dye that only crosses the cell membranes when they are damaged. The overall percentage of intact cells without PI stained nuclei was calculated relative to the total number of cells (Figure 7B). Targeted nanomaterials did not have a significant impact on plant cell membrane intactness. Both TP-β-CDs and TP-pATV1-SWCNTs maintained more than 93% of plant cells with intact membranes after 1 and 5 days of exposure, similar to controls without nanoparticles (Figure 7B). In addition, we performed identification of intact chloroplasts by differential interference contrast (DIC) microscopy as reported previously with some modifications.[67,68] Intact isolated chloroplasts observed by DIC microscopy have a highly reflective and continuous outer envelope, whereas damaged chloroplasts have a broken envelope with opaque and granular appearance (Figure 7C). The TP-β-CDs did not affect chloroplast membrane damage during the study period (Figure 7D). In contrast, the TP-pATV1-SWCNTs induced a significant decrease in chloroplast intactness after 1 day of exposure (Figure 7D). As proposed by the LEEP model, lipid exchange between SWCNT and chloroplast envelopes as the nanomaterials enter these organelles[22,23] could explain the temporary decrease in chloroplast membrane intactness. Our results indicate that high aspect ratio SWCNTs, but not CDs, result in significant disruption of plant lipid membrane structures.

Transient Increase in Leaf H_2O_2 Content after Nanomaterial Exposure. The impact of nanomaterials for targeted delivery of chemical cargoes and DNA on chloroplasts' reactive oxygen species (ROS) levels has not been explored. Chloroplasts are main sites for ROS generation.[65,69] We used a quantitative peroxide assay to monitor H_2O_2 content in leaves after treatment with targeted nanomaterials (Figure 8A) (Table S1). The TP-β-CDs and TP-pATV1-SWCNTs increased leaf H_2O_2 levels to 0.3225 ± 0.0190 and 0.2970 ± 0.0341 μmol gFW^{-1}, respectively, after 1 day of exposure, whereas control plants exhibited 0.0347 ± 0.0088 μmol gFW^{-1} values. The observed 10-fold increase in leaf H_2O_2 was within normal H_2O_2 levels reported for nonstressed land plants (<5 μmol gFW^{-1}).[70−74] However, H_2O_2 levels can vary significantly within plant species and even organs within plants.[70,71] Leaf H_2O_2 decreased to levels similar to controls (0.0320 ± 0.0021 μmol gFW^{-1}) after 5 days of exposure to TP-β-CDs (0.0583 ± 0.0033 μmol gFW^{-1}) and TP-pATV1-SWCNTs (0.0496 ± 0.0029 μmol gFW^{-1}) (Figure 8A). Although plants have mechanisms to catalytically scavenge ROS, the transient increase in the levels of leaf H_2O_2 could cause damage to DNA, chlorophyll pigments, and photosynthetic proteins.[73,75−78]

Oxidative Damage to Cell and Chloroplast DNA by targeted nanomaterials. To gain insight into the impact of targeted nanomaterials on plant cell and chloroplast genomes, we measured the relative 8-hydroxy-2′-deoxyguanosine (8-OHdG) levels in whole plant cell DNA and chloroplast DNA upon exposure to targeted nanomaterials (Table S1). Increased in ROS levels may result in DNA damage and the production

https://doi.org/10.1021/acsnano.2c02714
ACS Nano 2022, 16, 12156−12173

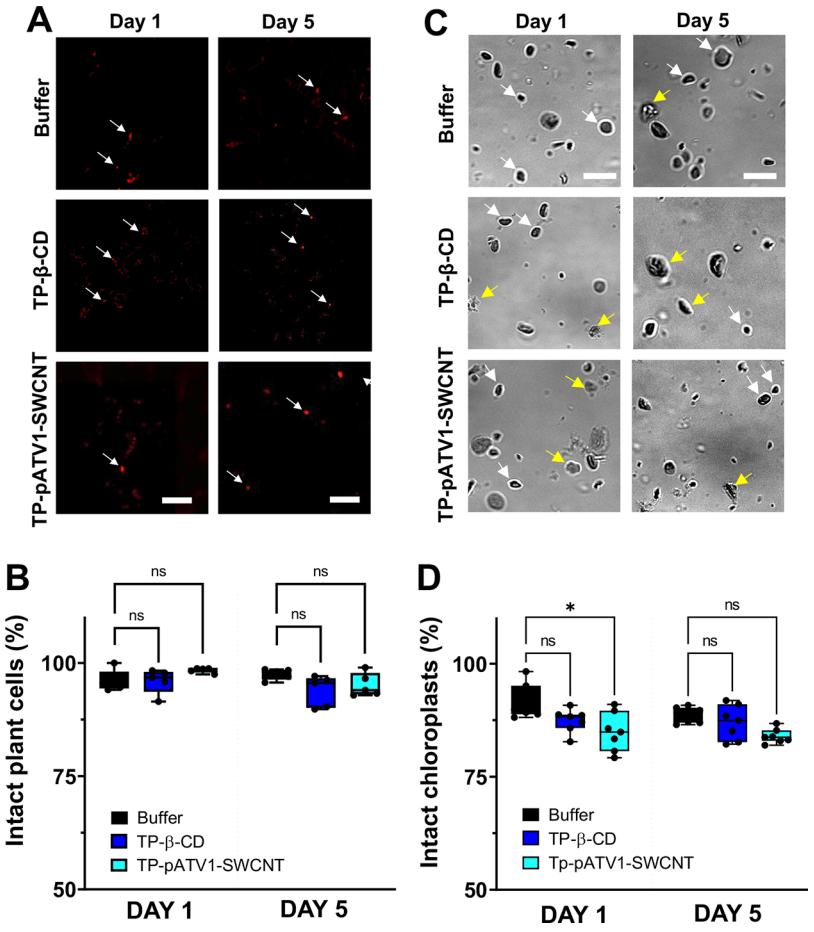


Figure 7. Impact of targeted nanomaterials on plant cell and chloroplast membrane integrity. (A) Confocal microscopy images of leaf mesophyll cell dead nuclei stained with PI. The PI a nonpermeable dye that can only cross plant cell membranes when they are damaged. White arrows point to selected stained nuclei. Scale bar 50 μm. (B) Quantitative analysis of the percentage of intact plant cells based on confocal microscopy imaging. Statistical analysis using one way ANOVA and post hoc Dunnett's test. No significant differences (ns), n = 5−7. (C) Bright-field microscopy images of isolated chloroplasts for intact chloroplast analysis. Intact chloroplasts exhibited a highly reflective and continuous outer membrane (white arrows) under DIC optical imaging. In contrast, the damaged chloroplasts showed broken outer membranes giving a granular appearance (yellow arrows). Scale bar 10 μm. (D) Quantitative analysis of the percentage of intact plant chloroplast membranes based on DIC optical imaging. Statistical analysis using one-way ANOVA and post hoc Tukey test. *p < 0.032, n = 5−7.

of 8-hydroxydeoxyguanosine (8-OHdG), a ubiquitous biomarker in the guanine of nucleic acids.[79,80] Significantly higher levels of 8-OHdG biomarkers in whole plant cell DNA were observed after 1 day of leaf exposure to TP-β-CD (14.9 ± 0.3 ng/mL) and TP-pATV1-SWCNT (15.5 ± 0.8 ng/mL) relative to controls without nanoparticles (9.7 ± 0.8 ng/mL) (Figure 8B). On day 5, the levels of 8-OHdG biomarkers remained slightly more elevated in both treatments with TP-β-CDs (14.9 ± 0.3 ng/mL) and TP-pATV1-SWCNTs (14.6 ± 0.4 ng/mL) relative to controls without nanoparticles (12.3 ± 0.9 ng/mL) (Figure 8B). In isolated chloroplast DNA samples from leaves treated with TP-pATV1-SWCNT, we also observed initial DNA oxidative damage on day 1 of exposure (14.7 ± 0.2 ng/mL), but after 5 days of exposure to the targeted nanomaterials, the 8-OHdG levels were similar to controls (TP-pATV1-SWCNT 13.2 ± 1.1 ng/mL; control 13.8 ± 0.9 ng/mL) (Figure 8C). In contrast, in leaves treated with TP-β-CDs, the levels of chloroplast 8OH-dG biomarkers 1 day after exposure (13.5 ± 1.0 ng/mL) were similar to that of controls without nanoparticles (12.6 ± 1.1 ng/mL) (Figure 8C). Accumulation of H_2O_2 may inhibit DNA repair mechanisms, allowing lesions and DNA damage in the plant nuclear genome to accumulate.[73,81] In contrast, plastid genomes such as those of chloroplasts are highly dynamic and contain hundreds of copies relative to the single nuclear genome in plant cells. If damaged plastid DNA exceeds the capacity of repairing mechanisms, the damaged DNA is fragmented and degraded, and new DNA is replicated.[82,83]

Effects of Targeted Nanomaterials on the Light and Carbon Reactions of Photosynthesis. ROS can damage chlorophyll pigments and reduce their biosynthesis in chloroplasts.[84] Chlorophyll is a marker for plant health status.[85,86] We determined the impact of targeted nanomaterials (Table S1) on chlorophyll content index (CCI) of *Arabidopsis* leaf tissues. After 1 day of exposure to targeted nanomaterials, the CCI of leaves interfaced with TP-β-CDs (35.5 ± 1.4) and TP-pATV1s (36.6 ± 3.0) was significantly lower than controls without nanoparticles (42.8 ± 1.7) (Figure 9A,B). A similar trend was observed in leaf CCI values after 5 days of exposure to TP-β-CDs (38.0 ± 2.8) and TP-pATV-SWCNTs (36.6 ± 2.5) and controls (46.3 ± 2.0) (Figure 9A,B). We verified that there is no interference in CCI

https://doi.org/10.1021/acsnano.2c02714
ACS Nano 2022, 16, 12156−12173

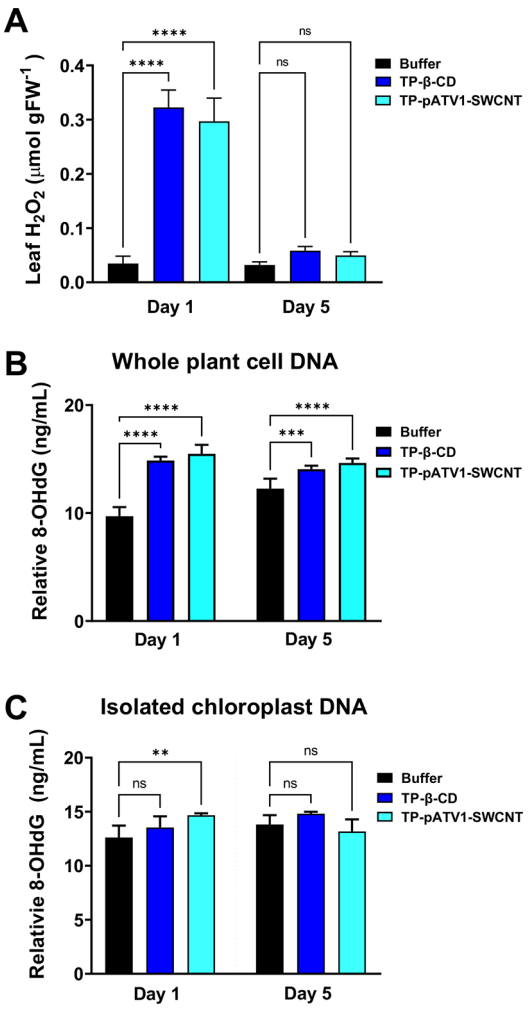


Figure 8. Oxidative stress in leaf mesophyll cells exposed to targeted nanomaterials. (A) Hydrogen peroxide (H_2O_2) content in *Arabidopsis* leaves treated with targeted nanostructures 1 and 5 days after exposure. Statistical analysis using two-way ANOVA and post hoc Tukey's test $n = 9$, * $p = <0.05$, ** $p < 0.0021$, **** $p < 0.0001$, $n = 3$. Quantitative assay of DNA damage caused by oxidative stress in (B) whole leaf cells and (C) isolated chloroplasts. The biomarker 8-OHdG was measured by ELISA, and the relative percentages of the 8-OHdG levels were compared to controls (buffer without nanoparticles) at 1 and 5 days after treatment with targeted nanostructures. Statistical analysis performed by one-way ANOVA and post hoc Tukey test ** $p <$ 0.0021, *** $p < 0.0002$, **** $p < 0001$, $n = 6$.

measurements with absorbance of the applied targeted nanomaterials by measuring leaf CCI before and after treatment with nanomaterials (Figure S6B). However, there were minimal signs of localized chlorosis or necrosis on plant leaves after treatment with targeted nanomaterials during this time frame (Figure S7). Previously, we reported no significant changes in chlorophyll content after the treatment with carboxylated, aminated, and amphiphilic CD at concentrations from 500 to 5000 mg/L[18] in crop plants (maize and cotton), indicating either a higher tolerance of crop plants to CDs or higher impact of targeted TP-β-CDs to chloroplasts on leaf health. The biocompatible concentration of nontargeted ssDNA coated semiconducting SWCNTs in *Arabidopsis* plants (5 mg/L)[87] was similar to that for TP-pATV1-SWCNTs (2 mg/L) used in this study for targeted delivery of plasmid DNA. However, the TP-pATV1-SWCNT induced a decline in leaf chlorophyll content after 5 days of exposure to the nanomaterials. Together, our results indicate that targeted delivery of TP-β-CDs and TP-pATV1-SWCNTs to chloroplasts in *Arabidopsis* plants can lead to the reduction in leaf chlorophyll content and that this effect on chloroplast pigments might be associated with a transient increase in ROS generation in leaves described above.

To assess the impact of TP-β-CD and TP-pATV1-SWCNTs on leaf photosynthesis, we measured carbon assimilation rates at varying photosynthetic active radiation levels (PAR). The photosynthesis light response curves provided information on the maximum leaf photosynthetic capacity (A_{max}) and photosystem II (PSII) quantum yield. The TP-β-CDs and TP-pATV1-SWCNTs did not influence carbon assimilation rates in the photosynthesis light-limited region (<400 μmol m^{-2} s^{-1} of photosynthetic active radiation, PAR) at day 1 and at day 5 (Figure 9C,D). However, we observed a reduction in A_{max} in the carboxylation limited region (>400 μmol m^{-2} s^{-1} PAR) at day 1 and day 5 relative to controls without nanoparticles (Figure 9C,D). Nanomaterials with high surface charge have been reported to form protein coronas in organisms.[88−91] The localization of nanomaterials in chloroplasts could result in photosynthetic protein adsorption onto the surface of the nanomaterials. The nanomaterial interactions with enzymes and substrates of the carbon reactions of photosynthesis may be responsible for the decline in maximum photosynthetic capacity. In contrast, the quantum yield of PSII was not impacted by targeted nanomaterials within a wide range of PAR levels from 1 one to 5 (Figure 9E,F). The maximum quantum yield of photosystem II (F_v/F_m) in dark-adapted leaves for controls (0.79 ± 0.02) (Figure 9E,F, inset) was similar to that of targeted nanomaterial treated plants at day 1 (0.79 ± 0.01, 0.80 ± 0.02) and at day 5 (0.79 ± 0.03, 0.80 ± 0.01) for TP-β-CDs and TP-pATV1-SWCNTs, respectively (Figure 9 E,F, inset). The F_v/F_m is a robust indicator of the maximum quantum yield of PSII chemistry.[92] A F_v/F_m value in the range of 0.79−0.84 is optimal for many plant species, with lowered values indicating plant stress.[93] Together these results indicate that targeted nanomaterials do not impact the light-dependent reactions of photosynthesis nor damage the photosystems or the chloroplast electron transport chain. However, the nanomaterial interactions with carboxylation reaction biomolecules may limit the leaf photosynthetic capacity.

CONCLUSIONS

We developed targeted carbon-based nanomaterials that deliver chemical cargoes (TP-β-CDs) and plasmid DNA (TP-pATV1-SWCNTs) to chloroplasts by plant biorecognition approaches. The application of targeted nanomaterials functionalized with guiding peptides as tools for plant bioengineering and precision agriculture relies on the understanding of their impact on plant function. Cell viability assays of plants treated with TP-β-CDs (20 mg/L) and TP-pATV1-SWCNTs (2 mg/L) indicated no significant differences in the percentage of dead cells compared to control plants after 5 days of exposure. The targeted nanomaterials did not affect cell membrane intactness. However, TP-pATV1-SWCNT induced a temporary disruption of isolated chloroplast envelopes where chloroplast guiding peptides are recognized by membrane translocon channels.[60,94,95] Because chloroplasts lack endocytosis-dependent mechanisms, nanoparticle uptake has been

https://doi.org/10.1021/acsnano.2c02714
ACS Nano 2022, 16, 12156−12173

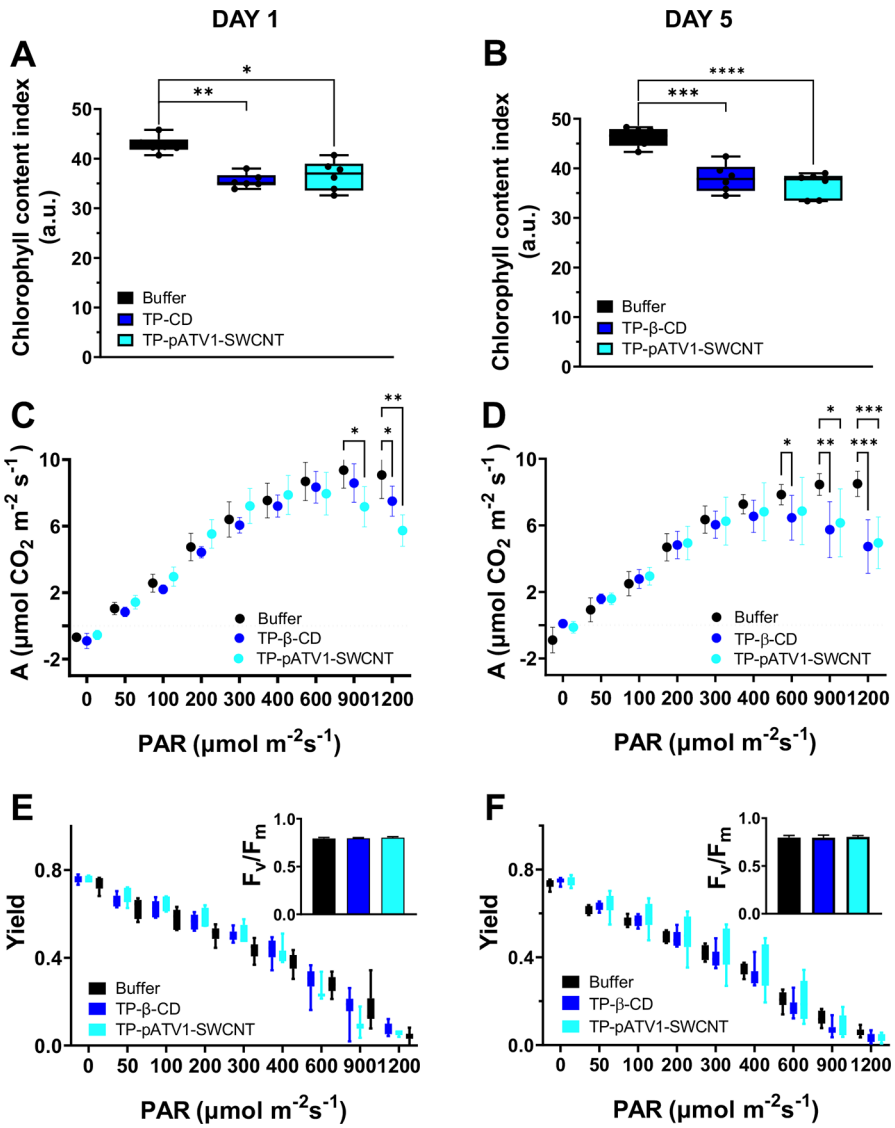


Figure 9. Effect of targeted carbon nanostructures on plant photosynthesis. Comparison of chlorophyll content index (SPAD) in *Arabidopsis* leaves treated with targeted nanomaterials at (A) day 1 and (B) day 5 after exposure. Statistical analysis was performed by one-way ANOVA and post hoc Tukey's test. * $p < 0.02$, ** $p < 0.0021$, *** $p < 0.0002$,** $p < 0.0001$, $n = 6$. Leaf carbon assimilation rates at varied photosynthetic active radiation (PAR) levels of *Arabidopsis* leaves at (C) day 1 and (D) day 5 after exposure to targeted nanomaterials. Statistical analysis was performed by two-way ANOVA and post hoc Dunnett's test. * $p < 0.02$, ** $p < 0.0021$, *** $p < 0.0002$,**** $p < 0.0001$, $n = 7-10$. Quantum yield of PSII and maximum efficiency of photosystem II (F_v/F_m) at (E) day 1 and (F) day 5 after exposure to targeted nanomaterials.**

proposed to occur by disruption of the organelle envelopes followed by self-rehealing of the lipid bilayers.[22,23] Exposure of plant leaf cells to targeted nanomaterials also induced a 10-fold transient increase in H_2O_2 levels relative to no nanoparticle controls. However, the leaf H_2O_2 content was within levels reported for healthy land plants.[70−74] Elevated H_2O_2 concentrations can lead to damage of biomolecules such as DNA, lipids, and proteins[81,96,97] and inhibit photosynthesis carboxylation rates in *Arabidopsis thaliana* plants.[70,98,99] We observed a 2-fold increase in oxidative damage to whole plant cell DNA after exposure with TP-β-CDs and TP-pATV1-SWCNTs. In contrast, isolated chloroplast DNA was not affected by TP-β-CDs, while TP-pATV1-SWCNTs induced transient oxidative damage. The chloroplasts genome is highly dynamic, and self-repairing mechanisms[82,83] could allow for rapid repair of damaged DNA or production of new DNA. A reduction in leaf chlorophyll content index levels after treatment with targeted nanomaterials could be attributed to increasing H_2O_2 levels.[73,75−78] Despite this effect on chlorophyll pigments, photosystem II health and quantum yields across a wide range of light levels remained unchanged, indicating no impact on the light reactions of photosynthesis. However, a reduction in maximum photosynthetic capacity was observed in the carboxylation limited region of photosynthesis. Interactions between the nanomaterial surface and photosynthetic proteins involved in carbon fixation and assimilation could be responsible for the decline in photosynthetic capacity.

This study demonstrates that carbon nanomaterials engineered with targeting peptides increase the delivery efficiency of chemical and plasmid DNA cargoes into chloroplasts by topical application of the leaf surface. CDs with molecular baskets could act as biocompatible,[29−31] degradable,[31,32] and traceable nanomaterials, made from

https://doi.org/10.1021/acsnano.2c02714
ACS Nano 2022, 16, 12156−12173

renewable resources,[18,33] for more precise delivery of active ingredients in crop plants, whereas pDNA-SWCNTs may enable transformation technologies for chloroplasts in plants in research facilities without the need of specialized equipment, tissue culture, or selection. Targeted nanomaterials overcome plant cell barriers including the cell wall, and lipid membranes, without mechanical aid, guided to chloroplasts by plant biorecognition. However, targeting of nanomaterials to the chloroplasts can induce transient increases in H_2O_2 levels that result in changes in whole leaf cell DNA and chlorophyll levels. Investigating scalable synthesis approaches, mechanisms of delivery, and safety of targeted carbon nanostructures will lead to sustainable nanotechnologies for improving agriculture. The results from this study provide insights for designing more efficient and biocompatible nanomaterials for plant research, agriculture, and environmental applications.

METHODS

Plant Growth. *Arabidopsis thaliana* plants were grown in Adaptis 1000 growth chambers (Conviron) under the following environmental conditions: 200 μmol m^{-2} s^{-1} PAR, 24 ± 1 and 21 ± 1 °C day/night, 60% humidity, and 14/10 h (day/night) regime. All plants were grown in (2.5 in. × 2.5 in. × 3 in.) pots filled with soil containing 1% marathon and 1% osmocote. Plants were watered once every 3 days. Three-week-old Columbia ecotype (Col-0) *Arabidopsis thaliana* plants (seed stock source CS60000) in the prebolting stage were used for this study.

Covalent Modification of SWCNT with Polyethylenimine Polymer. Oxidized SWCNTs (>90%, 652490-250MG, Sigma-Aldrich) were functionalized using a branched polyethylenimine (PEI) polymer (10,000 MW, 9002-98-6, Alfa Aesar). The PEI positive charge of the SWCNT surface allows the electrostatic grafting of negatively charged DNA and other biomolecules.[19,24,100] First, 20 mg of oxidized SWCNTs were dispersed into 100 mL of ultrapurified water and pH adjusted to 12 with NaOH. The SWCNT solution was bath sonicated for 30 min at 80 kHz and 390 W power at room temperature. The resulting SWCNT solution was slowly poured into a PEI aqueous solution (2 mg/mL) while stirring. The mixture of PEI and SWCNTs was stirred for 30 min before placing in a heat-resistant Falcon tube and incubating for 16 h at 85 °C in a mechanical oven (Isotemp, Fisher scientific). The resulting PEI-SWCNT was cooled to room temperature and then resuspended in 15 mL of molecular biology grade water (catalog # 46000CV Corning) and bath sonicated. All bath sonication steps were conducted for 30 min at 80 Khz and 390 W power at room temperature unless stated otherwise. The resulting suspension was centrifuged for 10 min at 4500 rpm (Allegra X-3R, Beckman Coulter) at room temperature to remove large agglomerates. The PEI-SWCNT was further purified with molecular biology grade water (catalog # 46000CV Corning) to remove excess PEI polymer by washing five times through an MWCO 100kD ultrafiltration microtube (VIVA SPIN 500, Sartorius). After each centrifugation step, PEI-SWCNTs were bath sonicated for 30 min to resuspend the nanomaterial pellet inside the VIVA SPIN 500 100kD column after each washing. The PEI-SWCNT solution was centrifuged six times in a microcentrifuge tube at 13.2 RCF for 1 h to remove any remaining agglomerates. The lack of a dark pellet after centrifugation steps is an indicator of well-dispersed suspensions of SWCNT.

The resulting PEI-SWCNT suspension was characterized by measuring the absorbance spectra on a UV−vis absorbance spectrophotometer (UV-2600, Shimadzu). The quality of the SWCNT suspension was determined by analyzing absorbance peaks at 632 nm. This measurement was performed with triplicates. The concentration of the PEI-SWCNT was determined spectrophotometrically using the absorption value at 632 nm and utilizing the equation (absorbance at 632 nm/extinction coefficient of 0.036) = mg L^{-1}. The final concentration obtained after purification ranged from 18 to 30 mg/L. The nanoparticle ζ potential was measured using a Zetasizer (Nano ZS, Malvern Instruments) in samples suspended in 10 mM TES buffer pH 7.0, with 0.1 mM NaCl. The hydrodynamic size was measured using Zetasizer (Nano ZS, Malvern Instruments) in samples suspended in a 10 mM TES buffer at pH 7.

Electrostatic Grafting of pATV1 Plasmid on PEI-SWCNT. Loading of pATV1 plasmid onto the PEI-SWCNT was performed by electrostatic grafting, which allows molecules with negative charge to electrostatic interact with positively charged surfaces on the PEI-SWCNT. We used previously reported electrografting methods[37,54] with some modifications. First, 0.01 mg of PEI-SWCNT with a net positive charge of 57.28 ± 1.86 mV was suspended in 1 mL of 10 mM TES buffer (7365-44-8, Sigma-Aldrich) at pH 7. 0.01 mg of positively charged PEI-SWNTs was mixed with 0.02 mg of negatively charged pATV1 DNA plasmid in a 10 mM TES buffer (pH 7.0). The final ratio of PEI-SWCNT to pATV1 plasmid DNA was 1:2 (PEI-SWCNT:pDNA), and the final concentrations of PEI-SWCNT and pATV1 plasmid were respectively 10 mg/L and 20 mg/L in 10 mM TES buffer (pH 7). The PEI-SWCNT coated in pATV1 plasmids was denoted pATV1-SWCNT. The pATV1-SWCNT solution was then bath sonicated at room temperature for 15 min at 80 kHz with no further purification steps. The characterization of the pATV1-SWCNT was determined by measuring the change in UV absorbance spectra, hydrodynamic diameter, and ζ potential (Malvern ZetaSizer).

Peptide Binding onto pATV1-SWCNTs. The pATV1-SWCNTs were functionalized with a chloroplast targeting peptide on their outer surface. The targeting peptide amino acid sequence was based on precursors of the conserved rubisco small subunit 1A (RbcS, genbank: OAP15425). Chloroplast targeting peptides have been utilized as a biorecognition motif that allows the import of nanomaterials and other nanoconjugates across the chloroplast membrane.[16,101] To improve the delivery of pATV1-SWCNT into chloroplasts, we designed a chloroplast targeting peptide with a lysine histidine (KH_6) polypeptide tail for enabling electrostatic binding to the plasmid DNA grafted onto the PEI-SWCNT (Figures 1 and 5A). Previous studies have reported lysine-histidine (KH_6) fusion peptides improve internalization of proteins and DNA into plant cells by destabilizing cell-membranes through electrostatic interaction between the protonated amino acids and the negatively charged cell membrane.[60,62,102] The chloroplast targeting peptide motif also contains a flexible linker of six glycine residues allowing increased stability in aqueous solutions and interaction with the biorecognition domains.[16,103] Synthesis of the chloroplast TP (MASSMLSSATMVGGGGGGKHKHKHKHKHKH) was performed by Genscript. The TP was diluted in a stock solution of 10 mg/L in phosphate-buffered saline (PBS) solution (pH 7). A 0.1 mg of chloroplast targeting peptide was added to 1 mL of pATV1-SWCNT suspension (2 mg/L). The mass ratio of PEI-SWCNT:DNA:TP was 1:2:50. The resulting TP-pATV1-SWCNT nanostructure was incubated for 15 min while stirring at room temperature, followed by a bath sonication on ice for 15 min at 80 kHz, and no further purification steps, then suspended in a 10 mM TES buffer (pH 7) for subsequent experiments.

pATV1 GFP-Expressing Plasmid. The pATV1 plastid encoding GFP was obtained from Pal Maliga's lab (UCR-MTA19-0083, Rutgers University) and Giga prepped by Genewiz. The pATV1 vector (Genbank accession MF461355) carries a dicistronic operon, a Prrn16 promoter driving expression of the two open reading frames (ORF) encoding the aadA spectinomycin resistance gene, and the second ORF encodes the GFP protein (Figure 5A).[43,104] The homologous recombination site flanking construct could enable insertion into the inverted repeat region of the plastid genome. Polycistronic mRNAs are not translated on the eukaryotic type 80S ribosomes in the cytoplasm. The dicistronic nature of pATV1 and its chloroplast codon optimization allow specific assessment of GFP expression in chloroplast genomes of plants treated with pATV1-SWCNT.

Carbon Dots Synthesis. CDs were synthesized by a solid-state reaction[18,33] using citric acid and urea. The CDs were further functionalized with a β-cyclodextrin molecular basket that enables chemical cargo loading into its cavity[35,105] and a terminal chloroplast

https://doi.org/10.1021/acsnano.2c02714
ACS Nano 2022, 16, 12156−12173

targeting peptide motif to import the nanomaterial containing a chemical cargo into chloroplasts.[16,101] Briefly, 2.40 g of urea (40 mmol) (CAS # 57-13-6, 99.2%, Fisher Chemical), 1.92 g of citric acid (10 mmol) (CAS # 77-92-9, 99.7%, Fisher Chemical), and 1.35 mL of ammonium hydroxide (10 mmol) ($NH_3 \cdot H_2O$, 30−33%, Sigma-Aldrich) were added into 2 mL of molecular biology grade water. The mixture was dissolved, placed into a 50 mL beaker, and incubated in a mechanical oven at 180 °C for 1 h and 20 min. Following this reaction, the resulting CD suspension was allowed to cool down at ambient temperature, dissolved in water, and stirred for 1 h. This CD solution was bath sonicated for 15 min at 80 kHz with intermittent mixing by pipetting. Then, the solution was centrifuged at 4000 rpm for 15 min to remove large particles and aggregates. The supernatant was then filtered using a centrifugal filter 10 K Amicon filter (catalog # UFC901024, Amicon ultra, Merck Millipore) at 4500 rpm for 30 min to wash out unreacted precursors and small molecules. This step was repeated five times. Lastly, the solution was filtered through a 0.22 μm filter membrane (catalog # 229757, CELLTREAT Scientific Products) to obtain purified CD.

Cyclodextrin Functionalized Carbon Dots. The resulting core CDs are functionalized with mono-(6-ethanediamine-6-deoxy)-β-cyclodextrin (β-CD, Cavcon) molecular baskets. The β-cyclodextrins allow the loading and delivery of chemical cargoes.[16,49] Synthesis of β-CD was adapted from previously reported methods[16,26,49] with some modifications. The CDs were diluted to 2 mg/L in a final volume of 10 mL using 10 mM TES buffer (pH 6.5). The CDs were sonicated for 30 min at 37 kHz and then filtered through a 20 nm filter (6809-1002, Anotop, Whatman). Then, 0.5 mg of *N*-hydroxysulfosuccinimide (NHS) and 0.2 mg 1-ethyl-3-(3-(dimethylamino)propyl) carbodiimide (EDC) were added to the solutions of CDs in 10 mM TES buffer (pH 6.5). The mixture was stirred for 30 min to activate carboxyl groups on the CDs. Following NHS/EDC activation, the solution 0.2 mg of 3-aminophenylboronic acid (APBA) was added dropwise to the reaction mixture and stirred at room temperature. Conjugation of APBA was allowed to react for 3 h at room temperature. The resulting APBA coated CDs were purified by washing three times with molecular biology grade water (catalog # 46000CV Corning) through a 10 K Amicon filter (catalog # UFC901024, Amicon ultra, Merck Millipore). Then, the APBA coated CDs were sonicated for 30 min and 37 kHz and filtered through a 20 nm filter (6809-1002, Anotop, Whatman). The pH of the resulting solution was adjusted to 10.5 with NaOH in the 10 mM TES buffer. A 0.35 mg of mono-(6-ethanediamine-6-deoxy)-β-cyclodextrin (Cavcon) was added to the solution and allowed to react overnight at room temperature while stirring. The resulting β-cyclodextrin functionalized CDs were denoted β-CDs and purified by washing at least twice with a 10 K Amicon filter (catalog # UFC901024, Amicon ultra, Merck Millipore), then sonicated for 30 min at 37 kHz. The resulting β-CDs were filtered through a 20 nm filter (catalog # 6809-1002, Anotop, Whatman).

β-Cyclodextrin CD Functionalization with Targeting Peptide. Chloroplast targeting peptides were covalently bonded to β-CD by a stepwise conjugation.[16,26] A double-ended cross-linker was used to attach β-CD to the targeting peptide. The succinimidyl-[(*N*-maleimidopropionamido)-tetraethylene glycol]ester (NHS-PEG4-MAL) (Thermo Fisher Scientific, USA) cross-linker contains chemical groups that are reactive to distinct functional groups located on the cyclodextrin molecule of the β-CD (terminal amine) and the targeting peptide's cysteine residue (sulfylhydrals). The 0.75 mg of NHS-PEG4-MAL linker was added to a solution of β-CD in a 10 mM TES buffer (pH 7.5). The mixture was incubated at room temperature for 1 h with stirring at 500 rpm. The excess NHS-PEG4-MAL was removed by washing the mixture through a 10 K Amicon filter (catalog # UFC901024, Amicon ultra, Merch Millipore) using molecular biology grade water (catalog # 46000CV Corning), and the product was suspended in a 10 mM TES buffer (pH 7.0). Lastly, 0.75 mg of the RbcS chloroplast targeting peptide (MASSMLS-SATMVGGC) was added to NHS-PEG4-MAL activated β-CDs and allowed to react for 1 h at room temperature while stirring. The RbcS peptide was dissolved in a 1 mL solution of 0.1% DMSO and 10 mM TES buffer (pH 7.0). The resulting chloroplast targeting CD (TP-β-CD) was washed three times using a 10 K Amicon filter (catalog # UFC901024, Amicon ultra, Merch Millipore) with molecular biology-grade water (catalog # 46000CV Corning).

Chemical Cargo Loading in β-Cyclodextrin Molecular Baskets. To show proof of the concept of targeted chemical delivery by TP-β-CD, we utilized a model fluorescent dye, 6-carboxyfluorescein (FDA), that can form inclusion complexes with β-cyclodextrins.[105−109] The FDA fluorescent dye has been reported to bind to the inner cavity of β-cyclodextrins and cyclodextrin derivatives for the investigation of chemical delivery by these molecular baskets in nonplant organisms.[34,110] The loading of FDA fluorescent cargoes onto β-CD nanomaterials was carried out by adding approximately 0.4 mg of FDA to an aqueous solution of 20 mg/L TP-CD (0.2 mg) in 10 mM TES buffer (pH 7.0). The mixture was vortexed and incubated for 0.5 h and washed to remove unbound molecules through a 10 K Amicon filter (catalog # UFC901024, Amicon ultra, Merch Millipore) in 10 mM TES buffer (pH 7.0).

Characterization of Nanomaterials. All nanomaterials were characterized by absorbance UV−vis spectroscopy (UV-2600 Shimadzu), hydrodynamic size (Nano S), and ζ potential (Nano ZS). The nanomaterial ζ potential and hydrodynamic diameter were measured in a 10 mM TES buffer (pH 7.0). The ζ potential measurements were performed in 0.1 mM NaCl to improve conductivity and analyzed by the Hückel approximation model.[111] CD fluorescence emission was collected using a fluorescence spectrometer (Horiba PTI QM-400). The stepwise synthesis of TP-β-CDs was analyzed using FTIR (Thermo Nicolet 6700 FTIR).

Nanomaterial Formulation and Topical Foliar Application. Nanomaterials were suspended in a 10 mM TES buffer (pH 7.0) with Silwet L-77 (Bio World) at a concentration used in agrochemical applications (0.1% v/v). The Silwet L-77 surfactant can reduce surface tension allowing rapid uptake into leaf stomatal pores and increase permeability in the epidermal layer through partial removal of the cuticular layer.[18] Each formulation of nanomaterials was loaded into a 5 mL spray bottle allowing foliar application to the whole plant. Approximately 0.3 mL of the solution was dispensed with each foliar application. For all experiments, each plant replicate (5−12 plants) was treated with three foliar sprays of nanomaterials suspended in the formulation (Table S1) and allowed to interact with leaves for 1, 5, or 7 days. The amount of nanomaterials sprayed on plant leaves was estimated by weighing *Arabidopsis* plants on Petri dishes before and after foliar application of the formulation (Figure S8). This experiment indicated that 34.2% of the total volume sprayed (900 μL) remains on the plant leaves. Thus, the amount of nanomaterials applied to plant leaves is β-CD (6.2 μg), TP-β-CD (6.2 μg), pATV1-SWCNT (0.62 μg), and TP-pATV1-SWCNT (0.62 μg).

Confocal Fluorescence Microscopy. *Arabidopsis* leaf samples were imaged by laser scanning confocal microscopy (TCS SP5, Leica Microsystems, Germany) using an ×40 wet objective (Leica Microsystems, Germany). Samples were dissected and mounted on glass slides inside a premade well of observation gel (Carolina). Confocal imaging of CDs (CD, β-CD, and TP-β-CD) and chloroplast autofluorescence were performed under 405 nm laser excitation (15% power) with an emission detection range set to 500−520 nm and 720−780 nm, respectively. The focal plane depth was set by adjusting the pinhole size to 3 airy units. To visualize the localization of chemical cargoes delivered by targeted CD complexes, a fluorescent 6-carboxyfluorescein dye (FDA, Invitrogen, catalog # C1360) was loaded into β-CDs and TP-β-CDs. The loading concentration of FDA to CDs was 2:1 as reported previously for β-cyclodextrins.[34,105,109] The fluorescein dye was excited separately by a 488 nm laser at 40% power with a PMT emission detection range of 525−550 nm, and the pinhole size was set to 3 airy units. For confocal analysis of TP-CY3-ds$(GT)_{15}$-SWCNTs and CY3-ds$(GT)_{15}$-SWCNTs, the CY3 dye covalently linked to the DNA oligo (CY3-GTGTGTGTGTGTGTGTGTGTGTGTGTGT). The double-stranded oligo containing CY3 fluorophore was used to image the DNA-SWCNT in plant cells and chloroplasts. The CY3 labeled DNA oligo (CY3-GTGTGTGTGTGTGTGTGTGTGTGTGTGT)

https://doi.org/10.1021/acsnano.2c02714
ACS Nano 2022, 16, 12156−12173

was purchased from IDT and annealed to a complementary DNA strand using the following procedure. An equal molar solution of each single stranded oligo was added to a tube containing 100 mM potassium acetate, 30 mM HEPES, pH 7.5 TBE buffer. The equal molar mixture was incubated at 95 °C for 5 min and allowed to cool gradually in a thermocycler for annealing of the complementary oligos. The CY3 dye covalently linked to the DNA oligo was excited by a 543 nm laser (40% power) and photomultiplier tube (PMT) emission detection range set to 550−590 nm and the focal plane pinhole size to 3 airy units. For imaging GFP in plant leaves, confocal microscopy settings were 488 nm laser excitation and 500−530 nm fluorescence emission detection. The focal plane pinhole size was set to 3 airy units.

Real-Time Quantitative PCR Analysis. Expression analysis was performed on 3-week-old *Arabidopsis* leaves treated with 2 mg/L pATV1-SWCNTs, TP-pATV1-SWCNTs, and controls without nanoparticles in 10 mM TES buffer (pH 7.0). Leaf RNA was extracted after 3 h of incubation with nanomaterials, 1, 5, and 7 days after treatment. The RNA was isolated using the Quick-RNA Plant Miniprep Kit (ZYMO). To digest any residual plasmid DNA carried over from into RT-qPCR reaction, samples were treated twice with DNase I enzyme (Zymo), while on the RNA plant miniprep column prep and after RNA was isolated. A 25 ng of purified RNA was added to Luna Universal One-Step RT-qPCR (NEB) reaction master mix per manufacturer's instructions. A quantitative real-time RT-qPCR was performed on a Bio-Rad CFX Connect Real-Time ThermalCycler (Bio-Rad). The relative expression levels of GFP genes were analyzed by the $2^{-\Delta\Delta CT}$ method.[63] The gene Actin2 (AT3G18780) was used as internal housekeeping control. Expression analysis primers were designed with the Primer3 version 4.1.0 tool using pATV1 sequence as a template (Figure S9A).[43,104,112] The primers sets (Table S2) were validated for assessing gene expression (Figure S9B).

Quantification of GFP by Enzyme-Linked Immunosorbent Assay. Leaf tissues treated with targeted TP-pATV1-SWCNTs and nontargeted pATV1-SWCNTs were ground under liquid nitrogen to a fine powder and homogenized in protein extraction buffer (50 mm Tris-HCl, pH 7.5, 150 mm NaCl, 0.1% [v/v] Triton X-100 and protease inhibitor cocktail). Total soluble proteins (TSP) were separated by centrifugation (12,000*g*) for 15 min. The amount of GFP protein in TSP was measured using the GFP enzyme-linked immunosorbent assay kit (Cell Biolabs, San Diego, CA, USA) according to the protocol provided by the manufacturer.

Statistical Analysis. We employed multiple strategies for statistical analysis depending on the number of variables and independent groups and whether comparisons were done for treatments with controls or across all treatments. Independent sample *t* tests were used to compare the means of two independent groups (i.e., Figures 3C and 5D). One-way ANOVA was performed to compare means of one variable across three or more independent groups (i.e., Figures 4C, 7B,D, 8, and 9A,B). Two-way ANOVA was performed to compare means of multiple treatments across several days (i.e., Figures 5E and 9C−F). Tukey's post hoc tests were used to compare every mean with every other mean (i.e., Figure 4C). Dunnet's post hoc test was used to compare every mean to a control mean (i.e., Figures 6 and 7B,D).

ASSOCIATED CONTENT

Supporting Information

The Supporting Information is available free of charge at https://pubs.acs.org/doi/10.1021/acsnano.2c02714.

FTIR spectra of step-by-step synthesis of targeted CD nanostructures, control confocal microscopy images of *Arabidopsis* leaf mesophyll cells without nanoparticles, imaging and fluorescence emission of TP-*β*-CD cargo delivery experiments, control confocal microscopy images of *Arabidopsis thaliana* leaf mesophyll cells exposed to PEI-SWCNT, leaf chlorophyll content index (CCI), primer design and efficiency testing for expression analysis, images of 3-week-old *Arabidopsis thaliana* plants exposed to targeted nanomaterials after 1 and 5 days incubation, and list of primer sequences used for RT-qPCR. Methods for plant cell viability assays, chloroplast isolation, intact chloroplast analysis, leaf H_2O_2 quantification assay, DNA extraction from isolated leaves and chloroplasts, 8-OHdG DNA damage biomarker assay, chlorophyll measurements, photosynthesis assays (PDF)

AUTHOR INFORMATION

Corresponding Author

Juan Pablo Giraldo − *Department of Botany and Plant Sciences, University of California-Riverside, Riverside, California 92521, United States;* orcid.org/0000-0002-8400-8944; Email: juanpablo.giraldo@ucr.edu

Authors

Israel Santana − *Department of Botany and Plant Sciences, University of California-Riverside, Riverside, California 92521, United States*

Su-Ji Jeon − *Department of Botany and Plant Sciences, University of California-Riverside, Riverside, California 92521, United States;* orcid.org/0000-0002-5917-8837

Hye-In Kim − *Department of Botany and Plant Sciences, University of California-Riverside, Riverside, California 92521, United States*

Md Reyazul Islam − *Department of Botany and Plant Sciences, University of California-Riverside, Riverside, California 92521, United States*

Christopher Castillo − *Department of Botany and Plant Sciences, University of California-Riverside, Riverside, California 92521, United States*

Gail F. H. Garcia − *Department of Botany and Plant Sciences, University of California-Riverside, Riverside, California 92521, United States*

Gregory M. Newkirk − *Department of Microbiology and Plant Pathology, University of California-Riverside, Riverside, California 92521, United States*

Complete contact information is available at: https://pubs.acs.org/10.1021/acsnano.2c02714

Author Contributions

J.P.G. and I.S. conceived and designed the experiments. I.S. performed nanomaterial synthesis and in vivo experiments. S.J. and H.K. contributed to nanomaterial synthesis and characterization. C.C. contributed with photosynthesis measurements. G.F.H.G. contributed with DNA extractions and DNA damage assays experiments. M.R.I. performed GFP ELISA analysis. G.N. contributed by working on primer validation and RT-qPCR data analysis. I.S., S.J., and J.P.G. analyzed data sets. Statistical analysis was performed by I.S. All authors contributed to reading and editing the manuscript. The manuscript was written by I.S. and J.P.G. with contributions from all authors.

Notes

The authors declare the following competing financial interest(s): This work is related to a U.S. patent (US11186845B1) entitled Compositions comprising a nanoparticle, a molecular basket comprising cyclodextrin, and a chloroplast-targeting peptide and methods of use thereof where Juan Pablo Giraldo, Israel Santana, Greg Newkirk are

https://doi.org/10.1021/acsnano.2c02714
ACS Nano 2022, 16, 12156−12173

inventors. Specific aspects of the manuscript are covered in the patent and include methods for targeted delivery of nanomaterials to chloroplasts using rationally designed guiding peptides and application of gene delivery to chloroplast using PEI functionalized single-walled carbon nanotubes with guiding peptides.

ACKNOWLEDGMENTS

This work was supported by the NSF grant no. 1911763 and USDA grant no. 2019-67013-29104 to J.P.G. The University of California, Riverside Dissertation Year Award fellowship supported I.S. We are grateful to Pal Maliga's group for providing the pATV1 plasmid for chloroplast expression analysis.

REFERENCES

(1) Alexandratos, N.; Bruinsma, J. World Agriculture towards 2030/2050: The 2012 Revision. *ESA Working Paper no. 12-03*; Food and Agriculture Organization of the United Nations: Rome, 2012.
(2) Ray, D. K.; Mueller, N. D.; West, P. C.; Foley, J. A. Yield Trends Are Insufficient to Double Global Crop Production by 2050. *PLoS One* **2013**, *8* (6), No. e66428.
(3) Kah, M.; Tufenkji, N.; White, J. C. Nano-Enabled Strategies to Enhance Crop Nutrition and Protection. *Nat. Nanotechnol.* **2019**, *14* (6), 532−540.
(4) United States EPA. *Climate Impacts on Agriculture and Food Supply*; United States Environmental Protection Agency: Washington, DC, 2016.
(5) Schlenker, W.; Lobell, D. B. Robust Negative Impacts of Climate Change on African Agriculture. *Environ. Res. Lett.* **2010**, *5* (1), 014010.
(6) Willett, W.; Rockström, J.; Loken, B.; Springmann, M.; Lang, T.; Vermeulen, S.; Garnett, T.; Tilman, D.; DeClerck, F.; Wood, A.; Jonell, M.; Clark, M.; Gordon, L. J.; Fanzo, J.; Hawkes, C.; Zurayk, R.; Rivera, J. A.; De Vries, W.; Majele Sibanda, L.; Afshin, A.; Chaudhary, A.; Herrero, M.; Agustina, R.; Branca, F.; Lartey, A.; Fan, S.; Crona, B.; Fox, E.; Bignet, V.; Troell, M.; Lindahl, T.; Singh, S.; Cornell, S. E.; Srinath Reddy, K.; Narain, S.; Nishtar, S.; Murray, C. J. L. Food in the Anthropocene: The EAT-Lancet Commission on Healthy Diets from Sustainable Food Systems. *Lancet* **2019**, *393* (10170), 447−492.
(7) Mba, C.; Guimaraes, E. P.; Ghosh, K. Re-Orienting Crop Improvement for the Changing Climatic Conditions of the 21st Century. *Agriculture & Food Security* **2012**, *1* (1), 7.
(8) Lowry, G. V.; Avellan, A.; Gilbertson, L. M. Opportunities and Challenges for Nanotechnology in the Agri-Tech Revolution. *Nat. Nanotechnol.* **2019**, *14* (6), 517−522.
(9) Newkirk, G. M.; de Allende, P.; Jinkerson, R. E.; Giraldo, J. P. Nanotechnology Approaches for Chloroplast Biotechnology Advancements. *Front. Plant Sci.* **2021**, *12*, 1496.
(10) Hofmann, T.; Lowry, G. V.; Ghoshal, S.; Tufenkji, N.; Brambilla, D.; Dutcher, J. R.; Gilbertson, L. M.; Giraldo, J. P.; Kinsella, J. M.; Landry, M. P.; Lovell, W.; Naccache, R.; Paret, M.; Pedersen, J. A.; Unrine, J. M.; White, J. C.; Wilkinson, K. J. Technology Readiness and Overcoming Barriers to Sustainably Implement Nanotechnology-Enabled Plant Agriculture. *Nature Food* **2020**, *1* (7), 416−425.
(11) Wang, J. W.; Grandio, E. G.; Newkirk, G. M.; Demirer, G. S.; Butrus, S.; Giraldo, J. P.; Landry, M. P. Nanoparticle-Mediated Genetic Engineering of Plants. *Mol. Plant* **2019**, *12* (8), 1037−1040.
(12) Giraldo, J. P.; Wu, H.; Newkirk, G. M.; Kruss, S. Nanobiotechnology Approaches for Engineering Smart Plant Sensors. *Nat. Nanotechnol.* **2019**, *14* (6), 541−553.
(13) Wang, D.; Saleh, N. B.; Byro, A.; Zepp, R.; Sahle-Demessie, E.; Luxton, T. P.; Ho, K. T.; Burgess, R. M.; Flury, M.; White, J. C.; Su, C. Nano-Enabled Pesticides for Sustainable Agriculture and Global Food Security. *Nat. Nanotechnol.* **2022**, *17*, 347−360.
(14) Servin, A. D.; White, J. C. Nanotechnology in Agriculture: Next Steps for Understanding Engineered Nanoparticle Exposure and Risk. *NanoImpact* **2016**, *1*, 9−12.
(15) Lv, J.; Christie, P.; Zhang, S. Uptake, Translocation, and Transformation of Metal-Based Nanoparticles in Plants: Recent Advances and Methodological Challenges. *Environmental Science: Nano* **2019**, *6* (1), 41−59.
(16) Santana, I.; Wu, H.; Hu, P.; Giraldo, J. P. Targeted Delivery of Nanomaterials with Chemical Cargoes in Plants Enabled by a Biorecognition Motif. *Nat. Commun.* **2020**, *11* (1), 2045.
(17) Wang, P.; Lombi, E.; Zhao, F.-J.; Kopittke, P. M. Nanotechnology: A New Opportunity in Plant Sciences. *Trends Plant Sci.* **2016**, *21* (8), 699−712.
(18) Hu, P.; An, J.; Faulkner, M. M.; Wu, H.; Li, Z.; Tian, X.; Giraldo, J. P. Nanoparticle Charge and Size Control Foliar Delivery Efficiency to Plant Cells and Organelles. *ACS Nano* **2020**, *14* (7), 7970−7986.
(19) Kwak, S.-Y.; Lew, T. T. S.; Sweeney, C. J.; Koman, V. B.; Wong, M. H.; Bohmert-Tatarev, K.; Snell, K. D.; Seo, J. S.; Chua, N.-H.; Strano, M. S. Chloroplast-Selective Gene Delivery and Expression in Planta Using Chitosan-Complexed Single-Walled Carbon Nanotube Carriers. *Nat. Nanotechnol.* **2019**, *14* (5), 447−455.
(20) Avellan, A.; Yun, J.; Zhang, Y.; Spielman-Sun, E.; Unrine, J. M.; Thieme, J.; Li, J.; Lombi, E.; Bland, G.; Lowry, G. V. Nanoparticle Size and Coating Chemistry Control Foliar Uptake Pathways, Translocation, and Leaf-to-Rhizosphere Transport in Wheat. *ACS Nano* **2019**, *13* (5), 5291−5305.
(21) Su, Y.; Ashworth, V.; Kim, C.; Adeleye, A. S.; Rolshausen, P.; Roper, C.; White, J.; Jassby, D. Delivery, Uptake, Fate, and Transport of Engineered Nanoparticles in Plants: A Critical Review and Data Analysis. *Environ. Sci.: Nano* **2019**, *6* (8), 2311−2331.
(22) Lew, T. T. S.; Wong, M. H.; Kwak, S.-Y.; Sinclair, R.; Koman, V. B.; Strano, M. S. Rational Design Principles for the Transport and Subcellular Distribution of Nanomaterials into Plant Protoplasts. *Small* **2018**, *14* (44), No. 1802086.
(23) Wong, M. H.; Misra, R. P.; Giraldo, J. P.; Kwak, S.-Y.; Son, Y.; Landry, M. P.; Swan, J. W.; Blankschtein, D.; Strano, M. S. Lipid Exchange Envelope Penetration (LEEP) of Nanoparticles for Plant Engineering: A Universal Localization Mechanism. *Nano Lett.* **2016**, *16* (2), 1161−1172.
(24) Demirer, G. S.; Zhang, H.; Matos, J.; Goh, N.; Cunningham, F. J.; Sung, Y.; Chang, R.; Aditham, A. J.; Chio, L.; Cho, M.-J.; Staskawicz, B.; Landry, M. P. High Aspect Ratio Nanomaterials Enable Delivery of Functional Genetic Material Without DNA Integration in Mature Plants. *Nat. Nanotechnol.* **2019**, *14*, 456−464.
(25) Spielman-Sun, E.; Avellan, A.; Bland, G. D.; Clement, E. T.; Tappero, R. V.; Acerbo, A. S.; Lowry, G. V. Protein Coating Composition Targets Nanoparticles to Leaf Stomata and Trichomes. *Nanoscale* **2020**, *12*, 3630−3636.
(26) Santana, I.; Hu, P.; Jeon, S.-J.; Castillo, C.; Tu, H.; Giraldo, J. P. Peptide-Mediated Targeting of Nanoparticles with Chemical Cargoes to Chloroplasts in Arabidopsis Plants. *Bio Protoc* **2021**, *11* (12), No. e4060.
(27) Marmiroli, M.; Mussi, F.; Pagano, L.; Imperiale, D.; Lencioni, G.; Villani, M.; Zappettini, A.; White, J. C.; Marmiroli, N. Cadmium Sulfide Quantum Dots Impact Arabidopsis Thaliana Physiology and Morphology. *Chemosphere* **2020**, *240*, 124856.
(28) Majumdar, S.; Pagano, L.; Wohlschlegel, J. A.; Villani, M.; Zappettini, A.; White, J. C.; Keller, A. A. Proteomic, Gene and Metabolite Characterization Reveal the Uptake and Toxicity Mechanisms of Cadmium Sulfide Quantum Dots in Soybean Plants. *Environmental Science: Nano* **2019**, *6* (10), 3010−3026.
(29) Li, Y.; Xu, X.; Wu, Y.; Zhuang, J.; Zhang, X.; Zhang, H.; Lei, B.; Hu, C.; Liu, Y. A Review on the Effects of Carbon Dots in Plant Systems. *Materials Chemistry Frontiers* **2020**, *4* (2), 437−448.
(30) Li, W.; Zheng, Y.; Zhang, H.; Liu, Z.; Su, W.; Chen, S.; Liu, Y.; Zhuang, J.; Lei, B. Phytotoxicity, Uptake, and Translocation of Fluorescent Carbon Dots in Mung Bean Plants. *ACS Appl. Mater. Interfaces* **2016**, *8* (31), 19939−19945.

https://doi.org/10.1021/acsnano.2c02714
ACS Nano 2022, 16, 12156−12173

(31) Swift, T. A.; Fagan, D.; Benito-Alifonso, D.; Hill, S. A.; Yallop, M. L.; Oliver, T. A. A.; Lawson, T.; Galan, M. C.; Whitney, H. M. Photosynthesis and Crop Productivity Are Enhanced by Glucose-Functionalised Carbon Dots. *New Phytol.* **2021**, *229* (2), 783−790.
(32) Li, H.; Huang, J.; Liu, Y.; Lu, F.; Zhong, J.; Wang, Y.; Li, S.; et al. Enhanced RuBisCO Activity and Promoted Dicotyledons Growth with Degradable Carbon Dots. *Nano Res.* **2019**, *12*, 1585−1593.
(33) Khan, W. U.; Wang, D.; Zhang, W.; Tang, Z.; Ma, X.; Ding, X.; Du, S.; Wang, Y. High Quantum Yield Green-Emitting Carbon Dots for Fe(III) Detection, Biocompatible Fluorescent Ink and Cellular Imaging. *Sci. Rep.* **2017**, *7* (1), 14866.
(34) Zhu, X.; Sun, J.; Wu, J. Study on the inclusion interactions of β-cyclodextrin and its derivative with dyes by spectrofluorometry and its analytical application. *Talanta* **2007**, *72* (1), 237−242.
(35) Saha, S.; Roy, A.; Roy, K.; Roy, M. N. Study to Explore the Mechanism to Form Inclusion Complexes of β-Cyclodextrin with Vitamin Molecules. *Sci. Rep.* **2016**, *6*, 35764.
(36) Zhang, H.; Zhang, H.; Demirer, G. S.; González-Grandío, E.; Fan, C.; Landry, M. P. Engineering DNA Nanostructures for siRNA Delivery in Plants. *Nat. Protoc.* **2020**, *15* (9), 3064−3087.
(37) Demirer, G. S.; Zhang, H.; Goh, N. S.; González-Grandío, E.; Landry, M. P. Carbon Nanotube-Mediated DNA Delivery without Transgene Integration in Intact Plants. *Nat. Protoc.* **2019**, *14*, 2954−2971.
(38) Jackson, C. T.; Wang, J. W.; González-Grandío, E.; Goh, N. S.; Mun, J.; Krishnan, S.; Geyer, F. L.; Keller, H.; Ebert, S.; Molawi, K.; Kaiser, N.; Landry, M. P. Polymer-Conjugated Carbon Nanotubes for Biomolecule Loading. *ACS Nano* **2022**, *16* (2), 1802−1812.
(39) Sanzari, I.; Leone, A.; Ambrosone, A. Nanotechnology in Plant Science: To Make a Long Story Short. *Frontiers in Bioengineering and Biotechnology* **2019**, *7*, 120.
(40) Begum, P.; Fugetsu, B. Phytotoxicity of Multi-Walled Carbon Nanotubes on Red Spinach (Amaranthus Tricolor L) and the Role of Ascorbic Acid as an Antioxidant. *J. Hazard. Mater.* **2012**, *243*, 212−222.
(41) Lin, S.; Reppert, J.; Hu, Q.; Hudson, J. S.; Reid, M. L.; Ratnikova, T. A.; Rao, A. M.; Luo, H.; Ke, P. C. Uptake, Translocation, and Transmission of Carbon Nanomaterials in Rice Plants. *Small* **2009**, *5* (10), 1128−1132.
(42) Tripathi, D. K.; Shweta; Singh, S.; Singh, S.; Pandey, R.; Singh, V. P.; Sharma, N. C.; Prasad, S. M.; Dubey, N. K.; Chauhan, D. K. An Overview on Manufactured Nanoparticles in Plants: Uptake, Translocation, Accumulation and Phytotoxicity. *Plant Physiol. Biochem.* **2017**, *110*, 2−12.
(43) Yu, Q.; Lutz, K. A.; Maliga, P. Efficient Plastid Transformation in Arabidopsis. *Plant Physiol.* **2017**, *175* (1), 186−193.
(44) Zhu, S.; Meng, Q.; Wang, L.; Zhang, J.; Song, Y.; Jin, H.; Zhang, K.; Sun, H.; Wang, H.; Yang, B. Highly Photoluminescent Carbon Dots for Multicolor Patterning, Sensors, and Bioimaging. *Angew. Chem., Int. Ed. Engl.* **2013**, *52* (14), 3953−3957.
(45) Holá, K.; Sudolská, M.; Kalytchuk, S.; Nachtigallová, D.; Rogach, A. L.; Otyepka, M.; Zbořil, R. Graphitic Nitrogen Triggers Red Fluorescence in Carbon Dots. *ACS Nano* **2017**, *11* (12), 12402−12410.
(46) Wang, T.; Wang, A.; Wang, R.; Liu, Z.; Sun, Y.; Shan, G.; Chen, Y.; Liu, Y. Carbon Dots with Molecular Fluorescence and Their Application as a "turn-Off" Fluorescent Probe for Ferricyanide Detection. *Sci. Rep.* **2019**, *9* (1), 10723.
(47) Wen, T.; Qu, F.; Li, N. B.; Luo, H. Q. A Facile, Sensitive, and Rapid Spectrophotometric Method for copper(II) Ion Detection in Aqueous Media Using Polyethyleneimine. *Arabian Journal of Chemistry* **2017**, *10*, S1680−S1685.
(48) Mazumdar, A.; Haddad, Y.; Milosavljevic, V.; Michalkova, H.; Guran, R.; Bhowmick, S.; Moulick, A. Peptide-Carbon Quantum Dots Conjugate, Derived from Human Retinoic Acid Receptor Responder Protein 2, against Antibiotic-Resistant Gram Positive and Gram Negative Pathogenic Bacteria. *Nanomaterials* **2020**, *10* (2), 325.
(49) Tang, C.; Qian, Z.; Huang, Y.; Xu, J.; Ao, H.; Zhao, M.; et al. A Fluorometric Assay for Alkaline Phosphatase Activity Based on β-Cyclodextrin-Modified Carbon Quantum Dots through Host-Guest Recognition. *Biosensors and Bioelectronics* **2016**, *83*, 274−280.
(50) Li, Y.; Pan, X.; Xu, X.; Wu, Y.; Zhuang, J.; Zhang, X.; Zhang, H.; Lei, B.; Hu, C.; Liu, Y. Carbon Dots as Light Converter for Plant Photosynthesis: Augmenting Light Coverage and Quantum Yield Effect. *J. Hazard. Mater.* **2021**, *410*, 124534.
(51) Mondal, S.; Purkayastha, P. α-Cyclodextrin Functionalized Carbon Dots: Pronounced Photoinduced Electron Transfer by Aggregated Nanostructures. *J. Phys. Chem. C* **2016**, *120* (26), 14365−14371.
(52) Kranjc, E.; Mazej, D.; Regvar, M.; Drobne, D.; Remškar, M. Foliar Surface Free Energy Affects Platinum Nanoparticle Adhesion, Uptake, and Translocation from Leaves to Roots in Arugula and Escarole. *Environ. Sci.: Nano* **2018**, *5* (2), 520−532.
(53) Xia, X.; Shi, B.; Wang, L.; Liu, Y.; Zou, Y.; Zhou, Y.; Chen, Y.; Zheng, M.; Zhu, Y.; Duan, J.; Guo, S.; Jang, H. W.; Miao, Y.; Fan, K.; Bai, F.; Tao, W.; Zhao, Y.; Yan, Q.; Cheng, G.; Liu, H.; Jiao, Y.; Liu, S.; Huang, Y.; Ling, D.; Kang, W.; Xue, X.; Cui, D.; Huang, Y.; Cui, Z.; Sun, X.; Qian, Z.; Gu, Z.; Han, G.; Yang, Z.; Leong, D. T.; Wu, A.; Liu, G.; Qu, X.; Shen, Y.; Wang, Q.; Lowry, G. V.; Wang, E.; Liang, X.-J.; Gardea-Torresdey, J.; Chen, G.; Parak, W. J.; Weiss, P. S.; Zhang, L.; Stenzel, M. M.; Fan, C.; Bush, A. I.; Zhang, G.; Grof, C. P. L.; Wang, X.; Galbraith, D. W.; Tang, B. Z.; Offler, C. E.; Patrick, J. W.; Song, C.-P. From Mouse to Mouse-ear Cress: Nanomaterials as Vehicles in Plant Biotechnology. *Explorationen* **2021**, *1* (1), 9−20.
(54) Demirer, G. S.; Zhang, H.; Matos, J. L.; Goh, N. S.; Cunningham, F. J.; Sung, Y.; Chang, R.; Aditham, A. J.; Chio, L.; Cho, M.-J.; Staskawicz, B.; Landry, M. P. High Aspect Ratio Nanomaterials Enable Delivery of Functional Genetic Material without DNA Integration in Mature Plants. *Nat. Nanotechnol.* **2019**, *14* (5), 456−464.
(55) Hirayama, F.; Uekama, K. Cyclodextrin-Based Controlled Drug Release System. *Adv. Drug Delivery Rev.* **1999**, *36* (1), 125−141.
(56) Li, Q.; Ohulchanskyy, T. Y.; Liu, R.; Koynov, K.; Wu, D.; Best, A.; Kumar, R.; Bonoiu, A.; Prasad, P. N. Photoluminescent Carbon Dots as Biocompatible Nanoprobes for Targeting Cancer Cells in Vitro. *J. Phys. Chem. C* **2010**, *114* (28), 12062−12068.
(57) Amer Ridha, A.; Pakravan, P.; Hemati Azandaryani, A.; Zhaleh, H. Carbon Dots; the Smallest Photoresponsive Structure of Carbon in Advanced Drug Targeting. *J. Drug Delivery Sci. Technol.* **2020**, *55*, 101408.
(58) Alas, M. O.; Alkas, F. B.; Aktas Sukuroglu, A.; Genc Alturk, R.; Battal, D. Fluorescent Carbon Dots Are the New Quantum Dots: An Overview of Their Potential in Emerging Technologies and Nanosafety. *J. Mater. Sci.* **2020**, *55* (31), 15074−15105.
(59) Smith, A. M.; Gilbertson, L. M. Rational Ligand Design To Improve Agrochemical Delivery Efficiency and Advance Agriculture Sustainability. *ACS Sustainable Chem. Eng.* **2018**, *6* (11), 13599−13610.
(60) Ng, K. K.; Motoda, Y.; Watanabe, S.; Sofiman Othman, A.; Kigawa, T.; Kodama, Y.; Numata, K. Intracellular Delivery of Proteins via Fusion Peptides in Intact Plants. *PLoS One* **2016**, *11* (4), No. e0154081.
(61) Yoshizumi, T.; Oikawa, K.; Chuah, J.-A.; Kodama, Y.; Numata, K. Selective Gene Delivery for Integrating Exogenous DNA into Plastid and Mitochondrial Genomes Using Peptide-DNA Complexes. *Biomacromolecules* **2018**, *19* (5), 1582−1591.
(62) Chen, Q. R.; Zhang, L.; Stass, S. A.; Mixson, A. J. Co-Polymer of Histidine and Lysine Markedly Enhances Transfection Efficiency of Liposomes. *Gene Ther.* **2000**, *7* (19), 1698−1705.
(63) Pfaffl, M. W. A New Mathematical Model for Relative Quantification in Real-Time RT-PCR. *Nucleic Acids Res.* **2001**, *29* (9), No. e45.
(64) Livak, K. J.; Schmittgen, T. D. Analysis of Relative Gene Expression Data Using Real-Time Quantitative PCR and the 2-ΔΔCT Method. *Methods* **2001**, *25* (4), 402−408.

https://doi.org/10.1021/acsnano.2c02714
ACS Nano 2022, 16, 12156−12173

(65) Liu, Y.; Ren, D.; Pike, S.; Pallardy, S.; Gassmann, W.; Zhang, S. Chloroplast-Generated Reactive Oxygen Species Are Involved in Hypersensitive Response-like Cell Death Mediated by a Mitogen-Activated Protein Kinase Cascade. *Plant J.* **2007**, *51* (6), 941−954.
(66) Wang, J.-Z.; Dehesh, K. ER: The Silk Road of Interorganellar Communication. *Curr. Opin. Plant Biol.* **2018**, *45*, 171−177.
(67) Lilley, R. M.; Fitzgerald, M. P.; Rienits, K. G.; Walker, D. A. Criteria of Intactness and the Photosynthetic Activity of Spinach Chloroplast Preparations. *New Phytol.* **1975**, *75* (1), 1−10.
(68) Kubis, S. E.; Lilley, K. S.; Jarvis, P. Isolation and Preparation of Chloroplasts from Arabidopsis Thaliana Plants. *Methods Mol. Biol.* **2008**, *425*, 171−186.
(69) Asada, K. Production and Scavenging of Reactive Oxygen Species in Chloroplasts and Their Functions. *Plant Physiol.* **2006**, *141* (2), 391−396.
(70) Veljovic-Jovanovic, S.; Noctor, G.; Foyer, C. H. Are Leaf Hydrogen Peroxide Concentrations Commonly Overestimated? The Potential Influence of Artefactual Interference by Tissue Phenolics and Ascorbate. *Plant Physiol. Biochem.* **2002**, *40* (6), 501−507.
(71) Cheeseman, J. M. Hydrogen Peroxide Concentrations in Leaves under Natural Conditions. *J. Exp. Bot.* **2006**, *57* (10), 2435−2444.
(72) Černý, M.; Habánová, H.; Berka, M.; Luklová, M.; Brzobohatý, B. Hydrogen Peroxide: Its Role in Plant Biology and Crosstalk with Signalling Networks. *Int. J. Mol. Sci.* **2018**, *19* (9), 2812.
(73) Tripathi, D.; Nam, A.; Oldenburg, D. J.; Bendich, A. J. Reactive Oxygen Species, Antioxidant Agents, and DNA Damage in Developing Maize Mitochondria and Plastids. *Front. Plant Sci.* **2020**, *11*, 596.
(74) Cheeseman, J. M. Hydrogen Peroxide and Plant Stress: A Challenging Relationship. *Plant stress* **2007**, *1* (1), 4−15.
(75) Hung, K. T.; Kao, C. H. Hydrogen Peroxide Is Necessary for Abscisic Acid-Induced Senescence of Rice Leaves. *J. Plant Physiol.* **2004**, *161* (12), 1347−1357.
(76) Bieker, S.; Riester, L.; Stahl, M.; Franzaring, J.; Zentgraf, U. Senescence-Specific Alteration of Hydrogen Peroxide Levels in Arabidopsis Thaliana and Oilseed Rape Spring Variety Brassica Napus L. Cv. Mozart. *J. Integr. Plant Biol.* **2012**, *54* (8), 540−554.
(77) Das, K.; Roychoudhury, A. Reactive Oxygen Species (ROS) and Response of Antioxidants as ROS-Scavengers during Environmental Stress in Plants. *Front. Environ. Sci. Eng. China* **2014**, *2*, 53.
(78) Chi, Y. H.; Paeng, S. K.; Kim, M. J.; Hwang, G. Y.; Melencion, S. M. B.; Oh, H. T.; Lee, S. Y. Redox-Dependent Functional Switching of Plant Proteins Accompanying with Their Structural Changes. *Front. Plant Sci.* **2013**, *4*, 277.
(79) Valavanidis, A.; Vlachogianni, T.; Fiotakis, C. 8-Hydroxy-2' -Deoxyguanosine (8-OHdG): A Critical Biomarker of Oxidative Stress and Carcinogenesis. *J. Environ. Sci. Health C Environ. Carcinog. Ecotoxicol. Rev.* **2009**, *27* (2), 120−139.
(80) Chiou, C.-C.; Chang, P.-Y.; Chan, E.-C.; Wu, T.-L.; Tsao, K.-C.; Wu, J. T. Urinary 8-Hydroxydeoxyguanosine and Its Analogs as DNA Marker of Oxidative Stress: Development of an ELISA and Measurement in Both Bladder and Prostate Cancers. *Clin. Chim. Acta* **2003**, *334* (1), 87−94.
(81) Hu, J. J.; Dubin, N.; Kurland, D.; Ma, B. L.; Roush, G. C. The Effects of Hydrogen Peroxide on DNA Repair Activities. *Mutat. Res.* **1995**, *336* (2), 193−201.
(82) Kumar, R. A.; Oldenburg, D. J.; Bendich, A. J. Changes in DNA Damage, Molecular Integrity, and Copy Number for Plastid DNA and Mitochondrial DNA during Maize Development. *J. Exp. Bot.* **2014**, *65* (22), 6425−6439.
(83) Oldenburg, D. J.; Bendich, A. J. DNA Maintenance in Plastids and Mitochondria of Plants. *Front. Plant Sci.* **2015**, *6*, 883.
(84) Aarti, P. D.; Tanaka, R.; Tanaka, A. Effects of Oxidative Stress on Chlorophyll Biosynthesis in Cucumber (Cucumis Sativus) Cotyledons. *Physiol. Plant.* **2006**, *128* (1), 186−197.
(85) Mukherjee, S.; Chakraborty, A.; Mondal, S.; Saha, S.; Haque, A.; Paul, S. Assessment of Common Plant Parameters as Biomarkers of Air Pollution. *Environ. Monit. Assess.* **2019**, *191* (6), 400.
(86) Kalaji, H. M.; Jajoo, A.; Oukarroum, A.; Brestic, M.; Zivcak, M.; Samborska, I. A.; Cetner, M. D.; Łukasik, I.; Goltsev, V.; Ladle, R. J. Chlorophyll a Fluorescence as a Tool to Monitor Physiological Status of Plants under Abiotic Stress Conditions. *Acta Physiol. Plant* **2016**, *38* (4), 102.
(87) Giraldo, J. P.; Landry, M. P.; Faltermeier, S. M.; McNicholas, T. P.; Iverson, N. M.; Boghossian, A. A.; Reuel, N. F.; Hilmer, A. J.; Sen, F.; Brew, J. A.; Strano, M. S. Plant Nanobionics Approach to Augment Photosynthesis and Biochemical Sensing. *Nat. Mater.* **2014**, *13* (4), 400−408.
(88) Walkey, C. D.; Chan, W. C. W. Understanding and Controlling the Interaction of Nanomaterials with Proteins in a Physiological Environment. *Chem. Soc. Rev.* **2012**, *41* (7), 2780−2799.
(89) Foroozandeh, P.; Aziz, A. A. Merging Worlds of Nanomaterials and Biological Environment: Factors Governing Protein Corona Formation on Nanoparticles and Its Biological Consequences. *Nanoscale Res. Lett.* **2015**, *10*, 221.
(90) Liu, W.; Rose, J.; Plantevin, S.; Auffan, M.; Bottero, J.-Y.; Vidaud, C. Protein Corona Formation for Nanomaterials and Proteins of a Similar Size: Hard or Soft Corona? *Nanoscale* **2013**, *5* (4), 1658−1668.
(91) Borgatta, J. R.; Lochbaum, C. A.; Elmer, W. H.; White, J. C.; Pedersen, J. A.; Hamers, R. J. Biomolecular Corona Formation on CuO Nanoparticles in Plant Xylem Fluid. *Environ. Sci.: Nano* **2021**, *8* (4), 1067−1080.
(92) Genty, B.; Briantais, J.-M.; Baker, N. R. The Relationship between the Quantum Yield of Photosynthetic Electron Transport and Quenching of Chlorophyll Fluorescence. *Biochimica et Biophysica Acta (BBA) - General Subjects* **1989**, *990* (1), 87−92.
(93) Maxwell, K.; Johnson, G. N. Chlorophyll Fluorescence—a Practical Guide. *J. Exp. Bot.* **2000**, *51* (345), 659−668.
(94) Jarvis, P.; Soll, J. Toc, Tic, and Chloroplast Protein Import. *Biochim. Biophys. Acta* **2002**, *1590* (1−3), 177−189.
(95) Lee, D. W.; Jung, C.; Hwang, I. Cytosolic Events Involved in Chloroplast Protein Targeting. *Biochim. Biophys. Acta* **2013**, *1833* (2), 245−252.
(96) Nafees, M.; Fahad, S.; Shah, A. N.; Bukhari, M. A.; Maryam; Ahmed, I.; Ahmad, S.; Hussain, S. Reactive Oxygen Species Signaling in Plants. In *Plant Abiotic Stress Tolerance: Agronomic, Molecular and Biotechnological Approaches*; Hasanuzzaman, M.; Hakeem, K. R.; Nahar, K.; Alharby, H. F., Eds.; Springer International Publishing: Cham, 2019; pp 259−272.
(97) Watanabe, K.; Yamada, N.; Takeuchi, Y. Oxidative DNA Damage in Cucumber Cotyledons Irradiated with Ultraviolet Light. *J. Plant Res.* **2006**, *119* (3), 239−246.
(98) Claeys, H.; Van Landeghem, S.; Dubois, M.; Maleux, K.; Inzé, D. What Is Stress? Dose-Response Effects in Commonly Used in Vitro Stress Assays. *Plant Physiol.* **2014**, *165* (2), 519−527.
(99) Smirnoff, N.; Arnaud, D. Hydrogen Peroxide Metabolism and Functions in Plants. *New Phytol.* **2019**, *221* (3), 1197−1214.
(100) Ramos-Perez, V.; Cifuentes, A.; Coronas, N.; de Pablo, A.; Borrós, S. Modification of Carbon Nanotubes for Gene Delivery Vectors. *Methods Mol. Biol.* **2013**, *1025*, 261−268.
(101) Lee, D. W.; Lee, S.; Oh, Y. J.; Hwang, I. Multiple Sequence Motifs in the Rubisco Small Subunit Transit Peptide Independently Contribute to Toc159-Dependent Import of Proteins into Chloroplasts. *Plant Physiol.* **2009**, *151* (1), 129−141.
(102) Lakshmanan, M.; Kodama, Y.; Yoshizumi, T.; Sudesh, K.; Numata, K. Rapid and Efficient Gene Delivery into Plant Cells Using Designed Peptide Carriers. *Biomacromolecules* **2013**, *14* (1), 10−16.
(103) Chen, X.; Zaro, J. L.; Shen, W.-C. Fusion Protein Linkers: Property, Design and Functionality. *Adv. Drug Delivery Rev.* **2013**, *65* (10), 1357−1369.
(104) Yu, Q.; Barkan, A.; Maliga, P. Engineered RNA-Binding Protein for Transgene Activation in Non-Green Plastids. *Nat. Plants* **2019**, *5* (5), 486−490.
(105) Flamigni, L. Inclusion of Fluorescein and Halogenated Derivatives in.alpha.-,.beta.-, and.gamma.-Cyclodextrins: A Steady-

https://doi.org/10.1021/acsnano.2c02714
ACS Nano 2022, 16, 12156−12173

State and Picosecond Time-Resolved Study. *J. Phys. Chem.* **1993**, *97* (38), 9566−9572.
(106) Dong, H.; Li, Y.; Yu, J.; Song, Y.; Cai, X.; Liu, J.; Zhang, J.; Ewing, R. C.; Shi, D. A Versatile Multicomponent Assembly via *β*-Cyclodextrin Host-Guest Chemistry on Graphene for Biomedical Applications. *Small* **2013**, *9* (3), 446−456.
(107) Angelini, G.; Campestre, C.; Boncompagni, S.; Gasbarri, C. Liposomes Entrapping *β*-Cyclodextrin/ibuprofen Inclusion Complex: Role of the Host and the Guest on the Bilayer Integrity and Microviscosity. *Chem. Phys. Lipids* **2017**, *209*, 61−65.
(108) Brittain, H. G. Excited-State Optical Activity of a Cyclodextrin Inclusion Compound. *Chem. Phys. Lett.* **1981**, *83* (1), 161−164.
(109) Hamada, F.; Ishikawa, K.; Higuchi, Y.; Akagami, Y.; Ueno, A. Strong Binding between Acidic Guests and Fluorescein Modified -*γ*-Cyclodextrin via Hydrogen Bonding. *J. Inclusion Phenom. Mol. Recognit. Chem.* **1996**, *25* (4), 283−294.
(110) Li, Q.; Zhang, Y.; Jin, Y.; Yang, Q.; Du, J.; Li, Y. Fluorescent Magnetic Nanosensors for Zn 2+ and CN- in Aqueous Solution Prepared from Adamantane-Modified Fluorescein and *β*-Cyclodextrin-Modified Fe 3 O 4@ SiO 2 via Host-Guest Interactions. *RSC Adv.* **2015**, *5* (84), 68815−68821.
(111) Doane, T. L.; Chuang, C.-H.; Hill, R. J.; Burda, C. Nanoparticle *ζ* -Potentials. *Acc. Chem. Res.* **2012**, *45* (3), 317−326.
(112) Koressaar, T.; Remm, M. Enhancements and Modifications of Primer Design Program Primer3. *Bioinformatics* **2007**, *23* (10), 1289−1291.

Recommended by ACS

MoS_2 Nanosheets–Cyanobacteria Interaction: Reprogrammed Carbon and Nitrogen Metabolism
Si Chen, Lijuan Zhao, *et al.*
SEPTEMBER 27, 2021
ACS NANO
READ

Fusion Peptide-Based Biomacromolecule Delivery System for Plant Cells
Kenta Watanabe, Keiji Numata, *et al.*
APRIL 26, 2021
ACS BIOMATERIALS SCIENCE & ENGINEERING
READ

Quantum Light Emission from Coupled Defect States in DNA-Functionalized Carbon Nanotubes
Yu Zheng, Han Htoon, *et al.*
JUNE 01, 2021
ACS NANO
READ

Site-Specific Protein Conjugation onto Fluorescent Single-Walled Carbon Nanotubes
Vitalijs Zubkovs, Ardemis A. Boghossian, *et al.*
SEPTEMBER 18, 2020
CHEMISTRY OF MATERIALS
READ

Get More Suggestions >

https://doi.org/10.1021/acsnano.2c02714
ACS Nano 2022, 16, 12156−12173